A centronuclear myopathy-causing mutation in dynamin-2 perturbs the actin-dependent structure of dendritic spines leading to excitatory synaptic defects in a murine model of the disease.

Running title: Actin-dependent synaptic defects in dynamin-2-linked CNM

Jorge Arriagada-Diaz[1], Bárbara Gómez[2], Lorena Prado-Vega[1], Michelle Mattar-Araos[3], Marjorie Labraña-Allende[3], Fernando Hinostroza[4], Ivana Gajardo[5], María José Guerra-Fernández[6], Jorge A. Bevilacqua[7], Ana M. Cárdenas[6], Marc Bitoun[8], Alvaro O. Ardiles[6,9,10*], Arlek M. Gonzalez-Jamett[6,11*].

[1]Programa de Magister en Ciencias, Mención Neurociencia, Universidad de Valparaíso, Valparaíso, Chile.
[2] Programa de Magister en Ciencias Médicas, Mención Biología Celular y Molecular, Universidad de Valparaíso, Valparaíso, Chile.
[3] Escuela de Tecnología Médica, Facultad de Medicina, Universidad de Valparaíso, Valparaíso, Chile.
[4] Centro de Investigación de Estudios Avanzados del Maule, CIEAM, Vicerrectoría de Investigación y Postgrado, Universidad Católica del Maule, Talca, Chile
[5] Departamento de Biología Celular y Molecular, Facultad de Ciencias Biológicas, Pontificia Universidad Católica de Chile, Santiago, Chile.
[6]Centro Interdisciplinario de Neurociencia de Valparaíso, Universidad de Valparaíso, Valparaíso, Chile.
[7] Departamento de Neurología y Neurocirugía, Hospital Clínico Universidad de Chile and Departamento de Anatomía y Medicina Legal, Facultad de Medicina, Universidad de Chile, Santiago, Chile.
[8] Sorbonne Université, Inserm, Institut de Myologie, Centre de Recherche en Myologie, F-75013 Paris, France.
[9]Centro de Neurología Traslacional, Facultad de Medicina, Universidad de Valparaíso, Valparaíso, Chile.
[10]Centro Interdisciplinario de Estudios en Salud, Facultad de Medicina, Universidad de Valparaíso, Viña del Mar, Chile
[11] Escuela de Química y Farmacia, Facultad de Química y Farmacia, Universidad de Valparaíso, Valparaíso, Chile.

*correspondence should be addressed to Dr. Arlek M. Gonzalez-Jamett +56-32-2508203 arlek.gonzalez@uv.cl or Dr. Alvaro O. Ardiles +56-32-2507354 alvaro.ardiles@uv.cl

Abstract

Dynamin-2 is a large GTP-ase, member of the dynamin superfamily, that regulates membrane remodeling and cytoskeleton dynamics. In the mammalian nervous system dynamin-2 modulates synaptic vesicle (SV)-recycling at the nerve terminals and receptor-trafficking to and from postsynaptic densities (PSDs). Mutations in dynamin-2 cause autosomal dominant centronuclear myopathy (CNM), a congenital neuromuscular disorder characterized by progressive weakness and atrophy of distal skeletal muscles. Cognitive defects have also been reported in dynamin-2-linked CNM patients suggesting a concomitant impairment of the central nervous system. Here we addressed the mechanisms that lead to cognitive defects in dynamin-2-linked CNM using a knock-in mouse model that harbors the p.R465W mutation in dynamin-2, the most common causing CNM. Our results show that these mice exhibit reduced capability to learn and acquire spatial and recognition memory, impaired long-term potentiation of the excitatory synaptic strength and perturbed dendritic spine morphology, which seem to be associated with actin defects. Together, these data reveal for the first time that structural and functional synaptic defects underlie cognitive defects in the CNM context. In addition our results contribute to the still scarce knowledge about the importance of dynamin-2 at central synapses.

Introduction

Dynamin super-family (DSF) is a group of large GTP-ases that act as mechano-enzymes promoting membrane remodeling in several processes including exocytosis, endocytosis, intracellular trafficking and mitochondrial dynamics among others (Ferguson, et al., 2012; González-Jamett, et al., 2013; Lomash, et al., 2015; Arriagada-Diaz, et al., 2020). Classical dynamins are the best understood members of the DSF. In mammals, these are encoded by three different genes: *DNM1*, *DNM2* and *DNM3* located on chromosomes 9, 19 and 1, respectively (Newman-Smith, et al., 1997; Züchner, et al., 2005; Noakes, et al., 1999). Classical dynamins are composed by five highly conserved domains: an amino-terminal GTP-ase domain that binds and hydrolyze GTP, a middle structural domain, a PH-domain involved in lipid membrane interaction, a GTP-ase effector domain (GED) and an arginine- and proline-rich domain (PRD) that allows dynamin association with SH3-containing proteins (Praefcke, et al., 2004; Ferguson, et al., 2012; Antonny, et al., 2016; Singh, et al., 2017; Arriagada-Diaz, et al., 2020). These domains organize in three regions: a “bundle signaling element” (BSE) composed by helices from the GTP-ase domain and GED, a “stalk” composed by helices from the middle domain and GED, and a membrane-inserting “foot” formed by the PH domain (Chappie, et al., 2009; Faelber, et al., 2011; Ford, et al., 2011; Kong, et al., 2018). In response to the binding of GTP, the BSE convey conformational changes from the GTP-ase domain to the “stalk” promoting dynamin oligomerization in helical structures that enhance its GTP-ase activity and favor membrane scission (Hinshaw, et al., 1995; Warnock, et al., 1997; Antonny, et al., 2016). Dynamin assembly/disassembly cycles and GTP-ase activity also regulate the bundling of the actin cytoskeleton (Gu, et al., 2010; Zhang, et al., 2020; Lin, et al., 2020; Schiffer, et al., 2015a).
The three classical dynamins are expressed at the central nervous system (CNS) and play functions at the pre- and post-synapses (Arriagada-Diaz, et al., 2020). At the pre-synapses they support the endocytic recycling of synaptic vesicles (SVs), exerting differential roles depending on the pattern of neuronal activity (Tanifuji, et al., 2013). In this regard, dynamin-1 mediates SV recycling upon high-frequency stimulation but responding in a slow time window after the arrival of action potentials (APs); dynamin-3 works in a faster time window independent of the frequency of APs and dynamin-2 mediates SV resupply upon high-frequency stimulation with a fast kinetics (Tanifuji, et al., 2013).

At the postsynaptic level dynamin-2 is an important regulator of surface-membrane availability of neurotransmitter-receptors (Carroll, et al., 1999; Kabbani, et al., 2004; Bhatnagar, et al., 2000; Wang, et al., 2017). The latter appears to be especially relevant for glutamatergic excitatory synapses, as dynamin-2 modulate insertion (Jaskolski, et al., 2009), removal (Carroll, et al., 1999; Chowdhury, et al., 2006), and recycling (Lu, et al., 2007; Zheng, et al., 2015) of the α-amino-3-hydroxy-5-methyl-4-isoxazolepropionic acid (AMPA) receptor to and from PSDs.

Although the isoforms -1 and -3 are expressed at a more greater level than dynamin-2 at the CNS (Okamoto, et al., 2001), dynamin-2 seems to play a more critical role for synapse development (Ferguson, et al., 2009). In fact, while embryos of dynamin-1 and/or dynamin-3 knockout (KO) mice survive for weeks after born (Ferguson, et al., 2007; Raimondi, et al., 2011), the KO of dynamin-2 results in early embryonic lethality (Ferguson, et al., 2009).

Mutations in dynamin-2 cause autosomal dominant human diseases (Züchner, et al., 2005; Bitoun, et al., 2005; Tanabe, et al., 2009; Liu, et al., 2011; Koutsopoulos, et al., 2011; Böhm, et al., 2012; Sambuughin, et al., 2015; Ali, et al., 2019). Among them, mutations in the middle and PH domain of dynamin-2 cause the autosomal dominant form of centronuclear myopathy (CNM) a rare neuromuscular disorder clinically manifested by myalgia, fatigability, weakness, and progressive atrophy of distal skeletal muscles (Jeannet, et al., 2004; Fischer, et al., 2006; Böhm, et al., 2012). Cognitive deficiencies, manifested as learning disabilities and limited intelligent quotient, have also been reported in CNM patients (Jeannet, et al., 2004; Fischer, et al., 2006; Echaniz-Laguna, et al., 2007; Böhm, et al., 2012) although the mechanisms involved have never been described. Here we show that a knock-in (KI) mouse model bearing the CNM-causing p.R465W mutation in dynamin-2 (Durieux, et al., 2010; Durieux, et al., 2012) exhibit a deficient capability to learn and acquire spatial and recognition memory. These cognitive defects correlate with impaired hippocampal excitatory synaptic transmission and plasticity. Furthermore, reduced dendritic spine density and changes in spine morphology are also evident in the brain of these mice. This latter seem to rely on defects in the actin cytoskeleton organization. As the catalytic activity of dynamin-2 is an important regulator of the actin dynamics (Mooren, et al., 2009; Gu, et al., 2010; Yamada, et al., 2013; Yamada, et al., 2016; Lin, et al., 2020) and this is a mechanism affected in dynamin-2 linked CNM (González-Jamett, et al., 2017) these data strongly suggest that CNM-causing mutations perturb the synaptic role of dynamin-2, impacting on the actin-dependent dendritic-spine structure and consequently affecting synaptic transmission and cognitive functions.

Results

Impaired learning and memory in adult CNM-mice

As early learning disabilities and cognitive defects have been reported in dynamin-2-related CNM patients (Jeannet, et al., 2004; Fischer, et al., 2006; Echaniz-Laguna, et al., 2007; Böhm, et al., 2012) we first evaluated learning and memory in a murine model of CNM. This is a knock-in mouse harboring the p.R465W mutation located in the middle domain of dynamin-2, the most common mutation causing CNM (Durieux, et al., 2010; Durieux, et al., 2012). Heterozygous mice (HTZ) recapitulate most of the signs of the myopathy, starting at 1 month old (m.o) and progressing as the animal ages (Durieux, et al., 2010). In order to assay learning and memory capabilities, adult HTZ mice over 6 m.o and their age-matched wild type (WT) littermates were subjected to two different behavioral paradigms: the novel object recognition test (NOR) and the Barnes maze (BM). Whilst NOR is useful to evaluate recognition

memory (Ennaceur, et al., 1988), BM is used to measure the ability of mice to learn and remember a spatial location (Rizzo, et al., 2017; Negrón-Oyarzo, et al., 2015; Pitts, et al., 2018).

First, we performed the NOR test. A schematic representation of the test is shown in Figure 1a. As expected WT mice spent significantly more time exploring a novel object (N) than a familial object (F) along sessions (Figure 1b). However HTZ mice did not modify their preference between N and F (Figure 1b) suggesting defects in the recognition memory. Moreover, HTZ mice exhibited a significantly reduced recognition index (D1) compared to their WT littermates (Figure 1c) strongly suggesting a decline in the recognition memory in the CNM context.

Then we applied the BM test. A schematic representation of the test is shown in Figure 1d. WT and HTZ mice were trained during 4 days (training) to find and enter into a hidden scape box using spatial clues. On the fifth day a reversal phase started in which the position of the scape-box was changed but the visual clues were kept to evaluate memory flexibility. As shown in Figure 1e the latency to find and enter into the scape box was decreasing throughout the training sessions for both WT and HTZ mice. However, HTZ mice took a longer time than WT to access the scape box throughout the reversal phase (Figure 1f). In fact, on the last day of the reversal phase WT mice took on average 57.3 ± 18.2 s whereas, HTZ mice took 100.6 ± 20.5 s to end the test (Figure 1f). Remarkably the percentage of HTZ mice that completed the test at the last day of the reversal phase was significantly lower than WT mice (Figure 1g) suggesting defects in spatial memory flexibility. Importantly, these observations did not appear to be due to locomotion defects in HTZ mice as walking time percentage (Figure supplement S1a) and total distance traveled in an open-field arena (Figure supplement S1b) were not different between groups.

Together these data show that the DNM2-linked CNM mouse model shares cognitive impairment with CNM patients and represents a pertinent model to identify the underlying molecular mechanisms

Excitatory synaptic transmission and plasticity are defective in adult hippocampal slices from CNM-mice

Changes in neuronal activity induce modifications in the efficacy of the synaptic transmission; this is known as synaptic plasticity and the mechanisms regulating it are the basis of learning and memory (Shors, et al., 1997). As synaptic plasticity in the hippocampus is particularly important for memory formation (Lee, et al., 2011) and the most studied forms of synaptic plasticity are long-term potentiation (LTP) and long-term depression (LTD) of the synaptic strength at the CA3-to-CA1 synapses (Malenka, et al., 2004) we evaluated excitatory synaptic transmission and plasticity in hippocampal slices isolated from HTZ mice over 6 m.o and their age-matched WT littermates.

The strength of the basal excitatory synaptic transmission was estimated as the I/O relationship. Figure 2a schematizes the experimental configuration for electrophysiological field recordings in hippocampal slices. Figure 2b show representative I/O traces for WT and HTZ hippocampal slices. As shown in Figure 2c the I/O relationship was significantly impaired in HTZ compared to WT slices. HTZ slices exhibited significantly lower fEPSP slopes (Figure 2d) but significantly higher FV-amplitudes (Figure 2e) compared to the WT condition. To evaluate whether plasticity of the synaptic strength is also affected in the CNM-context we induced NMDAR-dependent LTP in WT and HTZ hippocampal slices by using a standard theta

burst stimulation (TBS) protocol that drives a compound-LTP, involving pre- and post-synaptic mechanisms (Bayazitov, et al., 2007). Whilst LTP induction relies on the activation of NMDAR- that requires both presynaptic glutamate release and post-synaptic depolarization (Citri, et al., 2008), LTP maintenance mainly relies on AMPAR trafficking at the PSDs (Anggono, et al., 2012a). As shown in Figure 3 the magnitude of the TBS-induced LTP was significantly reduced after 50 min of record in HTZ compared to WT hippocampal slices (Figures 3a and 3c) suggesting a role of dynamin-2 in the maintenance of the tetanus-induced LTP. Furthermore, the early potentiation of the synaptic response measured during the first 5 minutes after the application of TBS was also reduced in HTZ compared to WT slices (Figure 3b) suggesting that LTP-induction is also dependent on dynamin-2. To evaluate the presynaptic contribution to the defects observed in HTZ synapses we estimated a paired-pulse facilitation (PPF) index (Figure 3d-e). PPF is a form of short-term synaptic plasticity that occurs when two stimulation-pulses of similar intensities are given in rapid succession, causing the second synaptic response to be bigger than the first one (Zucker, et al., 2002). Facilitation appears to be due to an increased presynaptic Ca^{2+} concentration that leads to enhanced neurotransmitter-release probability (Zucker, et al., 2002). The PPF index was unchanged between HTZ and WT hippocampal slices (Figure 3d-e) suggesting that, although presynaptic mechanisms could operate in the CNM-context, those appear to be independent of the release probability. Hence, the p.R465W mutation in dynamin-2 seems to mainly affect post-synaptic mechanisms, impairing synaptic potentiation upon sustained neuronal activity. The main post-synaptic impact was confirmed by a chemically induced LTP using the NMDAR-agonist Glycine (chLTP) which activates NMDAR without mediating a presynaptic glutamate release (Lu, et al., 2001; Zhang, et al., 2014). Upon chLTP a significant reduction in the magnitude of synaptic potentiation was observed in HTZ compared to WT slices (Figure supplement S2). Interestingly, these postsynaptic mechanisms appear to predominantly affect excitatory synaptic transmission, as we observed similar differences between HTZ and WT slices when the TBS protocol was elicited in the presence of *picrotoxin* (*PTX*), a blocker of the GABAR-dependent inhibitory transmission (Figure supplement S3).

Like LTP, LTD is a relevant long-term synaptic plasticity phenomena also implicated in learning and memory (Malenka, et al., 2004; Citri, et al., 2008). We evaluated weather LTD is also affected in the CNM-context and observed a significant reduction in the LTD-magnitude in HTZ compared to WT slices (Figure supplement S4).

Altogether these data demonstrate that the excitatory synaptic transmission and plasticity are DNM2-dependent processes impaired in the CNM context.

Dendritic-spine morphology is perturbed in neurons from adult CNM-mice

Besides a functional excitatory synaptic plasticity that mainly relies on changes in AMPAR activity at the PSDs (Anggono, et al., 2012b) there is a structural plasticity involving morphological changes at dendritic spines. Dendritic spines are actin-enriched protrusions where occur most of the excitatory synapses (Bosch, et al., 2012). Their density, size and shape correlate with the degree of synapse maturity and functionality and undergo modifications upon synaptic plasticity. In this regard it has been demonstrated that LTP-induction increases dendritic spine density and promotes the transit towards a

202 mature-spine shape with higher head diameter leading to a higher head/spine length ratio (Matsuzaki,
203 et al., 2001; Okamoto, et al., 2009). On the contrary, LTD-induction reduces dendritic spine density and
204 leads to the shrinkage of pre-existing spines (Okamoto, et al., 2004). In order to evaluate whether the
205 defects in excitatory synaptic transmission and plasticity observed in HTZ slices were related to
206 structural defects in dendritic spines, we marked brains from 6 m.o WT and HTZ mice with a Golgi- -
207 staining and quantified dendritic spine density and morphology in hippocampal and cortical neurons.
208 Figures 4 and 5 summarize observations made on hippocampal and cortical pyramidal neurons,
209 respectively. The comparison of the mean morphological parameters revealed a significant reduction in
210 spine density (number of spines per 1 µm of dendritic shaft) in HTZ compared to WT hippocampal
211 neurons (Figure 4b). Although no significant differences were observed in the spine shape on average
212 (Figure 4c) HTZ hippocampal neurons tended to exhibit a lower percentage of filopodial-protrusions and
213 a higher percentage of stubby-like spines. To further evaluate dendritic spine structure, we quantified
214 the cumulative frequency of spine lengths, head diameters and head/length ratios. Remarkably,
215 although head diameters were not different between WT and HTZ hippocampal neurons (Figure 4d)
216 these latter exhibited a significantly higher frequency of shorter spines, producing a leftward shift in the
217 cumulative distribution curve compared to WT spines (Figure 4e). As a consequence of having shorter
218 dendritic spines, HTZ hippocampal neurons also exhibited a significantly higher head diameter/spine
219 length ratio compared to WT neurons (Figure 4f).
220 Similar to that observed in hippocampal neurons, HTZ cortical neurons exhibited a significantly lower
221 mean spine density (Figure 5b) and tended to show a lower proportion of filopodial-protrusions
222 compared to the WT condition (Figure 5c). Remarkably, cortical HTZ neurons exhibited a higher
223 frequency of spines with smaller heads (Figure 5d) and shorter lengths (Figure 5e) although the
224 head/length ratio was unchanged (Figure 5f).
225 Together, these data suggest that pyramidal neurons bearing the dynamin-2 p.R465W mutation may
226 undergo modifications in density, head width and length of dendritic spines.

227 ***Impaired F-actin organization in CNM-neurons***

228 As dendritic spine morphology critically depends on the underlying actin network (Okamoto, et al.,
229 2009; Hotulainen, et al., 2010; Matus, et al., 2000) and actin dynamics is significantly affected in the
230 CNM context (González-Jamett, et al., 2017) we next evaluated actin organization in WT and HTZ
231 neurons. Hippocampal neurons primary cultured from neonatal mice (P0) were fixed, stained with the F-
232 actin-binding toxin phalloidin-rhodamine-B and visualized by confocal microscopy. The phalloidin
233 fluorescence intensity inside dendritic spines was quantified as an estimation of the F-actin content. As
234 shown in Figure 6, the phalloidin-fluorescence intensity was significantly lower in HTZ compared to WT
235 dendritic spines (Figure 6a-b) suggesting defects in the underlying spine-actin network. Indeed, HTZ
236 cultured hippocampal neurons stained with phalloidin exhibited a significantly higher frequency of
237 longer spines and lower head/spine ratio compared to WT neurons (Figure c-e) supporting the idea that
238 actin-dependent dendritic spine features could be impaired in the CNM context. As the relative amounts
239 of filamentous (F-) and monomeric (G-) actin is a determinant factor influencing dendritic spine
240 remodeling (Okamoto, et al., 2009), we quantified the F/G actin ratio in the hippocampus and cortex of
241 WT and HTZ mice. Our results showed that the balance between the F- and G-actin is perturbed in
242 brains of HTZ compared to WT mice (Figure supplement S5) further suggesting that synaptic defects in
243 HTZ mice could rely on disturbances in the actin dynamics.
244 All together the results presented here demonstrate that dynamin-2 is an important regulator of the
245 excitatory synaptic transmission in the mammalian brain by modulating actin-dependent dendritic spine
246 structure. This dynamin-2 function appears to be perturbed by the p.R465W mutation, impairing
247 synaptic structure and function and consequently leading to cognitive defects in the CNM context.

Discussion

Dynamin-2 is a large GTP-ase, member of the dynamin superfamily, that regulates membrane remodeling and actin dynamics, orchestrating actin and membrane-based processes such as exocytosis (González-Jamett, et al., 2013; Shin, et al., 2018), endocytosis (Van der Bliek, et al., 1993; Damke, et al., 1994; Loerke, et al., 2009) and endosomal recycling (Nicoziani, et al., 2000) among others.

In the nervous system, dynamin-2 is expressed at the pre-and post-synaptic levels (Okamoto, et al., 2001). At the pre-synapses dynamin-2 participates in the endocytic recycling of SVs, allowing the resupply of the ready-releasable pool in response to high frequency neuronal activity (Tanifuji, et al., 2013). At the post-synapses dynamin-2 regulates the availability of neurotransmitter receptors at the surface membranes (Carroll, et al., 1999; Kabbani, et al., 2004; Bhatnagar, et al., 2001; Wang, et al., 2017). Of particular relevance for excitatory synaptic transmission is the role played by dynamin-2 in AMPAR trafficking. The GTP-ase activity of dynamin-2 is required for the insertion of AMPAR into spines, by mediating their lateral diffusion from dendritic shafts to PSDs (Jaskolski, et al., 2009). In addition, dynamin-2 GTP-ase activity has been implicated in the removal (Carroll, et al., 1999; Chowdhury, et al., 2006) and recycling (Lu, et al., 2007; Zheng, et al., 2015) of AMPARs from and to PSDs. Hence, as AMPAR mediates the majority of fast excitatory synaptic transmission in the mammalian brain (Anggono, et al., 2012a), dynamin-2 could play a key regulatory function, supporting synaptic transmission and plasticity. In agreement with this idea, pharmacological inhibition of dynamin´s GTP-ase activity with dynole 34-2 (Arriagada-Diaz, et al., 2020) or dynasore (Fa, et al., 2014) significantly reduces LTP in hippocampal slices. Here, we demonstrate that the CNM-causing p.R465W mutation negatively impacts on the synaptic function of dynamin-2, leading to defects in excitatory synaptic transmission and plasticity in the brain of HTZ mice. As dynamin-2 is mostly expressed at the post-synaptic level (Okamoto, et al., 2001) it is likely that these HTZ defects in synaptic transmission rely on post-synaptic mechanisms such as AMPAR trafficking. Indeed, we observed a reduction in the magnitude of LTP in HTZ slices when we induced potentiation both electrically as well as when we did it chemically with glycine. As the chLTP protocol elicits potentiation of the synaptic strength by directly activating NMDARs without mediating the presynaptic release of glutamate (Lu, et al., 2001; Zhang, et al., 2014), these results are consistent with major post-synaptic mechanisms underlying HTZ synaptic defects. In fact, the PPF index was unchanged between WT and HTZ hippocampal slices (Figure 3d). As PPF is an estimation of the neurotransmitter release probability (Zucker, et al., 2002) it is unlikely that the changes that we observed in excitatory synaptic transmission in HTZ hippocampal slices are related to changes in the glutamate release probability. This is agreement with a recent report of Moro and collaborators who found that dynamins are dispensable for synaptic vesicle exocytosis (Moro, et al., 2021).However, we cannot rule out presynaptic defects in the CNM context. The fact that the amplitude of the fiber volley was significantly higher in HTZ compared to WT slices (Figure 2) could mean that more presynaptic terminals are recruited in order to compensate a reduction in the SV releasable pool. As dynamins´s GTP-ase activity of dynamin-2 regulates SV recycling (Tanifuji, et al., 2013; Watanabe, et al., 2013; Cheung, et al., 2019) it is possible to visualize a scenario in which the p.R465W mutation in dynamin-2 affects the size of the SV releasable pool, impacting neurotransmission. More experiments are needed to address this possibility.

Regardless of whether defects were pre or post-synaptic, there was a significant impairment in synaptic transmission and plasticity in HTZ compared to WT brains. Congruently, HTZ mice exhibit a cognitive decline, manifested as defects in recognition and spatial memory which can be explained by perturbations in the synaptic function. In this regard, even though CNM primarily affects skeletal muscles (Romero, et al., 2011; González-Jamett, et al., 2017) learning disabilities and limited intelligent quotient have been reported in dynamin-2-linked CNM patients (Jeannet, et al., 2004; Fischer, et al., 2006; Echaniz-Laguna, et al., 2007; Böhm, et al., 2012). As we observed here in HTZ mice, cognitive

296 defects manifested by CNM patients could be due to disturbances in the synaptic function. Remarkably,
297 in addition to changes in the synaptic strength, we also observed structural modifications in dendritic
298 spines of the HTZ compared to WT neurons. In this regard, dendritic spine density was significantly
299 lower in pyramidal neurons from adult HTZ mice (Figures 4-5). As the majority of the synaptic contacts
300 between excitatory neurons are made on dendritic spines (Harris, et al., 1994) a net reduction in spine
301 density can lead to significant defects in synaptic transmission, such as those observed in HTZ
302 hippocampal slices. Moreover, dendritic spine morphology, which is closely related to the maturity and
303 functionality of synapses (Holtmaat, et al., 2009; Gipson, et al., 2017), also underwent modifications in
304 HTZ compared to WT neurons (Figures 4, 5 and 7). Although on average we did not observe significant
305 differences in spine morphology between genotypes, the cumulative distribution of the spine length,
306 spine head diameter and head/length ratio yielded important variations. Whilst mature HTZ
307 hippocampal neurons exhibited a higher frequency of shorter spines, neonatal hippocampal neurons
308 cultured from HTZ pups showed a higher frequency of immature larger spines with a significant
309 reduction in the head diameter/spine length ratio. Moreover, cortical neurons from adult HTZ brains
310 exhibited higher frequency of shorter spines, with smaller heads compared to WT neurons. As spines
311 with large head and large head/spine ratio have been found to correlate with an increased PSD area and
312 AMPAR density (Matsuzaki, et al., 2001) a reduction in spine head diameter or the head/length ratio
313 could explain defects in synaptic transmission and plasticity.
314 A major factor regulating spine morphology is the actin cytoskeleton (Okamoto, et al., 2004; Bosch, et
315 al., 2014). A dynamic F-actin network exists in dendritic spines, which acts primarily as a cytoskeleton
316 component defining spine architecture, but also as a scaffold for the recruitment of post-synaptic
317 proteins including AMPAR (Okamoto, et al., 2009; Cingolani, et al., 2008; Stefen, et al., 2016).Therefore,
318 remodeling of the spine-actin is critical for structural and functional synaptic plasticity (Kim, et al., 1999;
319 Okamoto, et al., 2004) and it is not surprising that perturbations in the actin dynamics lead to different
320 synaptopathies (Penzes, et al., 2012; Pelucchi, et al., 2020). In fact, the changes that we observed in the
321 density and shape of dendritic spines in HTZ neurons (Figures 4-6) are compatible with defects in actin
322 dynamics. In this regard, we previously demonstrated that the actin organization and remodeling are
323 disrupted in muscle cells of HTZ mice (González-Jamett, et al., 2017) suggesting that a similar
324 mechanism could operate in central synapses. Our results here suggest that an imbalance in the relative
325 amounts of F- and G-actin occurs in the brain of HTZ mice (Figure supplement S5) which could be
326 associated with a defective spine-actin dynamics. An increase in the F/G ratio as we observed in HTZ
327 compared to WT brains (Figure supplement S5) could be related to a less dynamic neuronal actin
328 network, with a reduced ability to remodel itself to support synaptic transmission. But, how the
329 p.R465W mutation could impact on dynamin-2 function leading to defects in actin and actin-based
330 mechanisms? The residue 465 localizes near to a putative direct actin-binding motif in dynamin-2 (Gu, et
331 al., 2010, red region in Figure 7a). As these authors proposed, unassembled dynamins could bind to
332 short actin filaments via their middle domain and in turn oligomerize in rings promoting actin
333 polymerization (Gu, et al., 2010; Gu, et al., 2014; Shiffer, et al., 2015). If that is true, the substitution of a
334 positive-charged arginine by a non-polar tryptophan in the oligomerization-middle domain of dynamin-2
335 could certainly influence its actin-binding properties affecting actin dynamics. In this regard, by using
336 full-atom and coarse-grained molecular simulations, we previously demonstrated that the p.R465W
337 mutation affects the interaction between the residue 465 and surrounding amino acids, modifying the
338 conformation of the BSE and consequently impacting on the GTPase-domain position and dynamin-2
339 self-assembly (Hinostroza, et al., 2020). Recent evidences suggest that helix of dynamin-2 interact with
340 F-actin via their outer-rim (Zhang, et al., 2020). This region includes the C-terminus PRD that is adjacent
341 to the GTPase domain and to the BSE (Figure 7b). It is noteworthy that the R/W 465 residue interacts
342 with the BSE in a region that is close to the starting point of the PRD (Figures 7b-c). As the p.R465W
343 mutation in dynamin-2 extends the angle between the G domain and the BSE (Hinostroza, et al., 2020)

344 in the tetramer and helical configuration (Figure 7d) we speculate that the arginine/tryptophan
345 substitution in the residue 465 not only modifies the BSE conformation but also changes the position of
346 the PRD, being able to affect the PRD-actin interaction. This assumption is in agreement with a model in
347 which the actin-remodeling activity of dynamin-2 is disrupted by CNM-causing mutations. In accordance
348 with this idea, Lin and collaborators recently demonstrated that dynamin-2 regulates the bundling of
349 actin at the postsynaptic membranes of neuromuscular junctions (NMJs). Remarkably, CNM-linked
350 mutations seem to disrupt this dynamin-2 function impairing actin remodeling and perturbing
351 postsynaptic structures at the NMJs (Lin, et al., 2020). A similar mechanism could be operating at central
352 excitatory synapses in the brain of HTZ mice, explaining the defects that we observed in dendritic spine
353 morphology, synaptic transmission and cognitive functions.

354 In our knowledge, this is the first report addressing the mechanisms that lead to cognitive defects in
355 dynamin-2-linked CNM. Our data support a model in which the actin cytoskeleton organization is
356 impaired, leading to structural and functional synaptic defects. In addition, our results contribute to the
357 better understanding of the still scarce knowledge about the function of dynamin-2 at central synapses.

358

359 **Methods**

360 *Animals*
361 HTZ mice harboring the p.R465W mutation in dynamin-2 is a mammalian model of CNM. These mice
362 recapitulate most of the CNM-signs, which start at 1 mo and progress as animals age (Durieux et al.,
363 2010). HTZ and WT littermates (C57BL/6 strain) were housed at room temperature with *ad libitum*
364 access to food and water. Mice were maintained on light-darkness cycles of 12–12 h, according to
365 standard protocols. Genotyping was performed by PCR as previously described (Durieux et al., 2010)
366 using DNA extracted from ears. Primers used were: 3'-CTGCGAGAGGAGACCGAGC-5' (forward) and 3'-
367 GCTGAGCACTGGAGAGTGTATGG-5 (reverse). PCR products were electrophorated in agarose gels and
368 bands of 445 bp and 533 bp, representing the WT and p.R465W mutated allele respectively, were
369 detected. All animal protocols described here were conducted in accordance with the approved
370 protocols of the Institutional committee for the care of laboratory animals of Universidad de Valparaíso
371 (BEA131-18).
372
373 *Behavioral tests*
374 Recognition and spatial learning and memory were assessed in 6 m.o WT and HTZ mice by application of
375 the Novel Object Recognition (NOR) test and the Barnes maze test (BM), respectively. Locomotion
376 capabilities in mice were evaluated by application of a standard Open Field (OF) test. All behavioral
377 tests were carried out in a room conditioned for this purpose, with controlled temperature (21 ° ± 2 ° C),
378 white noise (50 dB) and regulated luminosity (200 lux).
379 *NOR.* This test is based on the spontaneous tendency of rodents to spend more time exploring a novel
380 object than a familial one. Maze consisted of a 50 cm x 40 cm x 63 cm square white acrylic box in which
381 mice explored freely during 5 min throughout three phases: (i) sample, where mice explored a pair of
382 identical objects; (ii) retention, where mice were removed for cleaning and changing objects; and (iii)
383 choice, where mice explored a pair of different objects: a familiar object (F) and a new object (N). Each
384 session was repeated during 3 days. The time that mice spent exploring F or N was quantified. A
385 recognition index (D1) was calculated as [N exploration time-F exploration time.

386 *BM*. This task is dependent on the intrinsic inclination of rodents to escape from an aversive
387 environment (Barnes 1979). It consists in a 70 cm diameter white circular platform elevated 90 cm from
388 the floor with 20 equally spaced holes along the perimeter (each 7 cm in diameter) located 2 cm from
389 the edge of the platform. The animals are oriented by means of spatial clues located on the walls of the
390 room, in order to find and remember the position of a black plexiglass escape box (17 × 13 × 7 cm) that
391 is hidden under one of the holes. The maze was illuminated with 4 incandescent lights to produce a light
392 level of around 600 lux fall on the circular platform. BM test consisted of 9 session days, 4 trials per
393 session along which three phases were carried out: (i) pre-training phase, where mice were trained to
394 find the escape platform (ii) training phase, where mice remember the position of the escape box
395 guided by the spatial clues arranged in the room, (iii) reversion phase, where the location of the escape
396 box was changed but maintaining the position of the spatial clues to evaluate memory flexibility. In all
397 phases, if mice did not find the target hole and did not enter into the escape box during 3 minutes, the
398 test was terminated. Subsequently, the experimenter guided the animal to the escape box and allowed
399 it to remain in the box for 1 minute before returning to their holding box. Latency or time that took to
400 animals to find the target hole and enter into the scape box was quantified.
401 *OF.* Mice were placed in the center of a 50 cm x 40 cm x 63 cm white acrylic box and left to explore
402 freely during 5 minutes, along 3 sessions (1 session per day). Total distance traveled and the percentage
403 of walking time was quantified.
404
405 *Field electrophysiological recordings*
406 To evaluate basal strength of synaptic transmission and synaptic plasticity we evoked field excitatory
407 postsynaptic potentials (fEPSPs) in WT and HTZ hippocampal slices by stimulating the Schaffer
408 Collaterals (CA3) and recording the synaptic responses in *stratum radiatum* of CA1. Hippocampal slices
409 were prepared as previously described (Ardiles et al. 2014). Animals were euthanized under deep
410 anesthesia using isoflurane at saturation and their brains were quickly removed after craniotomy. Brains
411 were sectioned in two hemispheres, removing hippocampus to be sectioned in 300 µm thick slices and
412 immersed in dissection buffer (in mM: 212.7, sucrose 26 $NaHCO_3$, 1.23 NaH_2PO_4, 10 D-glucose, 5 KCl, 2
413 $CaCl_2$, 1 MgCl, 3 pyruvate) using vibratome (Vibratome 1000 plus, Ted Pella Inc., CA, USA). Slices were
414 transferred and kept for 1 hour at room temperature in artificial cerebrospinal fluid (ACSF, in mM: 124
415 NaCl, 26 $NaHCO_3$, 1.23 NaH_2PO_4, 10 D-glucose, 5 KCl, 2 $CaCl_2$, 1 MgCl, 3 pyruvate). All recordings were
416 obtained in an immersion chamber perfused with ACSF (30 ± 0.5°C; 2 ml / min). Stimulation was
417 performed with pulses of 0.2 ms duration, administered through concentric bipolar stimulation
418 electrodes. Basal responses were recorded using mean stimulation intensity compared to maximum.
419 Basal synaptic transmission was analyzed by determining input-output relationship (I /O) of the fEPSP
420 generated by gradually increasing the stimulation intensity. Input corresponded to the amplitude of the
421 fiber volley and the output to the initial slope of the fEPSP. To evaluate long-term potentiation (LTP),
422 slices were subjected to a high-frequency electrical stimulation protocol or a chemical stimulation
423 protocol. LTP using high-frequency electrical stimulation was performed using a standard theta burst
424 (TBS) protocol, which consists of 4 trains at 100 Hz for 1 min (Flores-Muñoz et al. 2020; Gajardo et al.
425 2018). On the other hand, chemical LTP (chLTP) was induced by perfusing a glycine solution (glycine, Gly
426 600 µM + *picrotoxin*, PTX 50 µM + strychnine Stric 3 µM) (X. Y. Zhang et al. 2014), directly on the
427 hippocampal slices during 5 minutes. Gly is co-agonist of NMDAR, PTX is an inhibitor of the inhibitory

428 GABAR-dependent transmission and Stric is an inhibitor of Gly-receptors. Once the application time of
429 solution had elapsed, it was removed and the registration buffer was replaced with a new one. In both
430 cases, fEPSPs were recorded for 20 minutes prior to stimulation and for 50 minutes after the application
431 of the electrical stimulus (TBS) or chLTP.
432 To assess long-term depression (LTD), a standard low-frequency electrical protocol was induced which
433 consists of a 1 Hz stimulation for 15 minutes (Gajardo et al. 2018). fEPSPs were recorded for 20 minutes
434 prior to stimulation and for 60 minutes after the application of LFS.
435 Paired pulse facilitation (PPF) was obtained by stimulating at different intervals in a range between 25-
436 300 ms and recording excitatory post-synaptic potential (EPSP). A PPF index was estimated by dividing
437 the amplitude of the second response over the first one (R2/R1).
438
439 *Spine density and morphology*
440 HTZ mice over 6 mo and age-matched WT littermates were sacrificed, brains were quickly removed and
441 processed using the FD Rapid Golgi-Stain-TM kit (FD Neuro Technologies) according to the manufacturer
442 instructions. Golgi impregnated cortical and hippocampal neurons were imaged using a Leica DM500
443 microscope equipped with a camera system, a 63X /1.40 oil (HCPL Apo, Leica) objective and the Leica
444 acquisition software. Pyramidal neurons were analyzed and processed using the ImageJ software (NIH,
445 USA). To evaluate the spine density and morphology, measurements were performed in dendritic
446 segments of 10 to 20 µm, visualized from four apical dendrites per neuron. Dendritic- protrusions were
447 categorized following the parameters revised by Risher and collaborators (Risher et al., 2014). Long, thin
448 without-head protrusions of more than 2 um long were classified as immature filopodia; wide-head
449 (>0.6 um width) and short protrusions (<1 um) were classified as mature mushroom-spines; wide-
450 head/without neck protrusions (length: width ratio <1 um) were classified as stubby-spines; thin and
451 short (<2 um) headed protrusions were classified as thin-spines. Cup-shaped protrussions were
452 classified as branched spines (Figure Supplement S6). Measurements were made by two different
453 experimenters, blind to the genotype of the samples.
454
455 *Neuron primary culture*
456 Hippocampal neurons were primary cultured from post-natal mice (P0) following the protocol described
457 by Beduoain and collaborators (Beduoain et al., 2012). Briefly, hippocampi from individual pups were
458 dissected, trypsinized for neurons dissociation and plated in poly-L-lysine treated coverslips and
459 maintained in medium containing B27-supplement (GIBCO), glutamax (GIBCO) and
460 Penicilin/Streptomycin mixture of antibiotics (GIBCO). Genotype of each single culture was confirmed a
461 *posteriori* from tail-segments of pups. 2 days after culture neurons were treated with 5µM cytosisne-
462 arabinoside (Ara-C) to inhibit the proliferation of non-neuronal cells. At 7 *DIV,* neurons were fixed with
463 4%PFA + 4% sucrose during 10 min at 37°C, permeabilized with 0.1% triton-X100 in saline phosphate
464 buffer (PBS, mM: 137 NaCl, 2.7 KCl, 10 Na_2HPO_4, 2 KH_2PO_4, pH 7.4) during 10 min at room temperature
465 and stained during 1 h with 1µM phalloidin-Rhodamin-B (Sigma) before confocal visualization. Images
466 were acquired in a confocal microscope (upright Eclipse Nikon 80i) using a 60x magnification objective.
467 Single confocal images were acquired with the EZ-C1 (Nikon) software using similar acquisition settings
468 between comparable samples. Analyses of dendritic spines stained with phalloidin were made with the
469 ImageJ software (NIH, USA) by two different experimenters, blind to the genotype of the samples. The
470 phalloidin fluorescence intensity was measured inside spines, without including the neighboring
471 dendritic shaft.
472
473

F/G actin assay

Hippocampal and cortical tissue from WT and HTZ mice were lysed and homogenized in conditions that stabilize filamentous (F-) and monomeric (G-) actin using an F/G actin commercial assay (Cytoskeleton Inc.). Lysed extracts were ultracentrifuged at 100,000 g for 1 h at 37 °C in order to separate pellets (F-actin) and soluble (G-actin) fractions. The F-actin pellet was resuspended in a depolymerizing buffer (Cytoskeleton Inc) and then F-and G-actin fractions were diluted in loading buffer (50 mM Tris–HCl, 2% SDS, 10% glycerol, 1% beta-mercaptoethanol and bromophenol blue). Samples were subjected to electrophoresis in 12%-SDS-PAGE, transferred to a PVDF membrane, blocked for 1 h with 5% non-fat milk in TBS-T (mM:150 NaCl, 50 Tris/HCl, pH 7.4, 0.05% Tween-20), incubated with a polyclonal antibody against actin (1:500; Cytoskeleton Inc.) and developed by chemiluminescence. Densitometric analysis of the F- and G-actin bands was performed with the ImageJ software.

Statistical analyses

GraphPad Prism 9 software was used to perform the statistical analyses. Paired or unpaired non-parametric Mann-Whitney test were used to compare WT and HTZ conditions. Two-way ANOVA followed by Bonferroni multiple comparison post-test was also used in electrophysiological experiments. Data in graphs represent the mean ± SEM, with a p-value <0.05 being significant. If not specified, differences were not statistically significant.

Declaration of Conflicting Interests

The author(s) declared no potential conflicts of interest with respect to the research, authorship, and/or publication of this article.

Acknowledgements

We thank Dr. Isaac García-Carrillo (Escuela de Odontología, Universidad de Valparaíso) for facilitating his laboratory for western blot development. This work was supported by the grants Fondecyt 11180731 (to AMG-J), Fondecyt 1201342 (to AOA), and ICM-ANID ICN09-022 CINV (to AMG-J, AOA, and AMCD) and by ANID scholarship 22200154 (to JA-D).

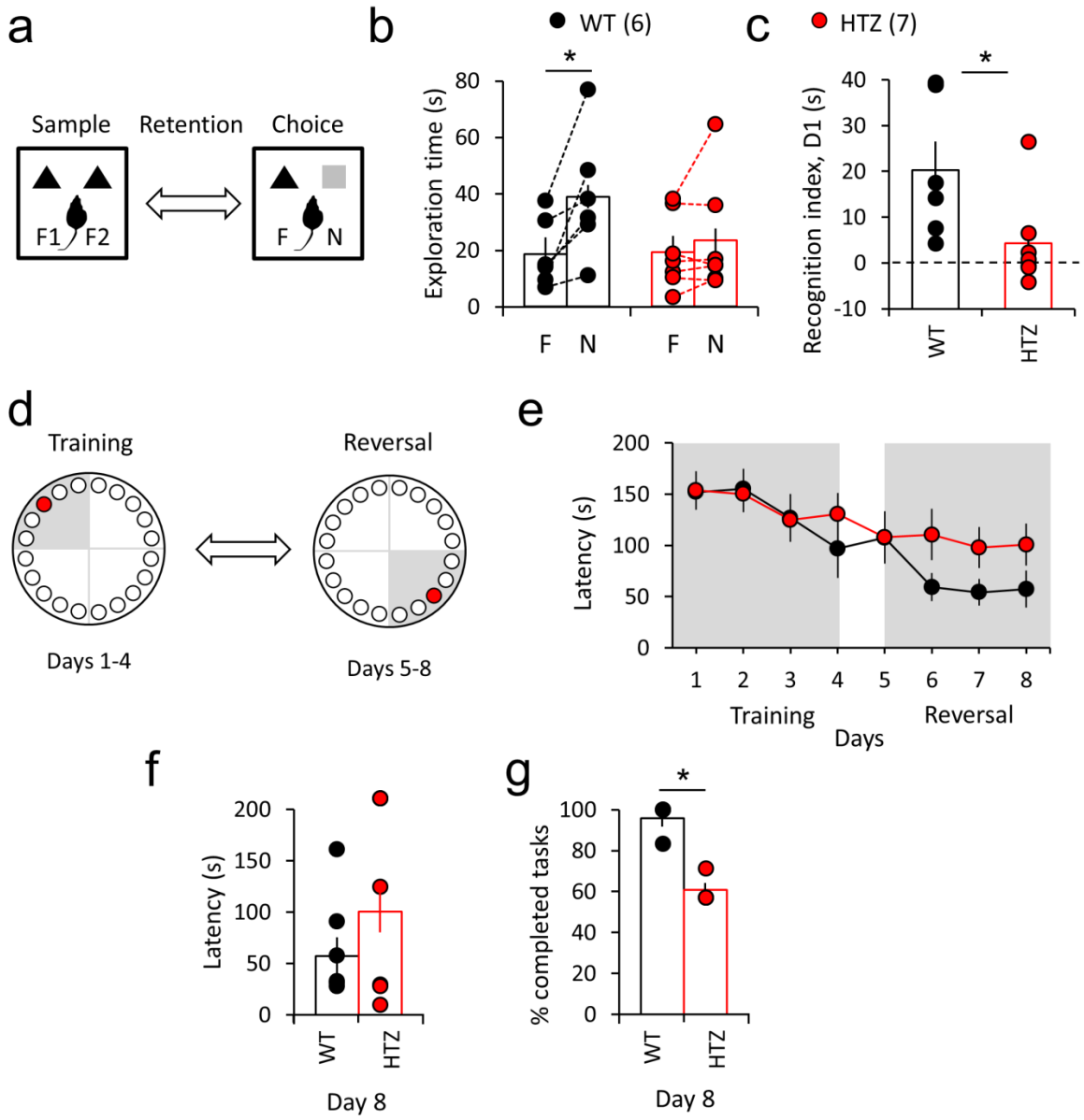

Figure 1: HTZ mice exhibit reduced performance in recognition and spatial memory tasks. WT (black circles) and HTZ (red circles) mice over 6 m.o were evaluated in the novel object recognition (NOR) and the Barnes maze tests to estimate recognition and spatial memory, respectively. **(a)** Representative scheme of the NOR test. Mice are faced with two identical objects (F1 and F2) in the sample phase and then in the choice phase, the objects are replaced by an extra copy of the familiar object (F) and a novel object (N). **(b)** Mean exploration time for familial (F) and novel (N) objects. Note that HTZ mice spend significantly less time exploring new objects compared to WT mice. Wilcoxon test, *p =0.0312 compared to the WT condition. **(c)** Mean recognition index (D1). Positive values indicate recognition of the novel over the familial object. Mann-Whitney test, *p =0.0221 compared to the WT condition **(d)** Schematic representation of the BM test. Mice were trained for 4 days to find and escape to a hidden dark box using visual cues (Training phase). On the fifth day, the escape box is located in the opposing quadrant keeping the visual cues to evaluate spatial memory flexibility (Reversal phase). **(e)** Quantification of the latency to entry into the escape box throughout the training and reversal sessions.

(f) Mean latency to entry into the escape box at day 8 of the test (last day of the reversal phase). **(6)** Quantification of the percentage of animals that completed the task at the end of the reversal phase. Note that the the time to enter into the escape box was not statistically significant, but the percentage of HTZ mice that completed the task on the last day of the reversal phase was significantly lower than WT. Mann-Whitney test, *p =0.0286 compared to the WT condition All data are represented as mean ± SEM. In parentheses is the number of WT and HTZ mice.

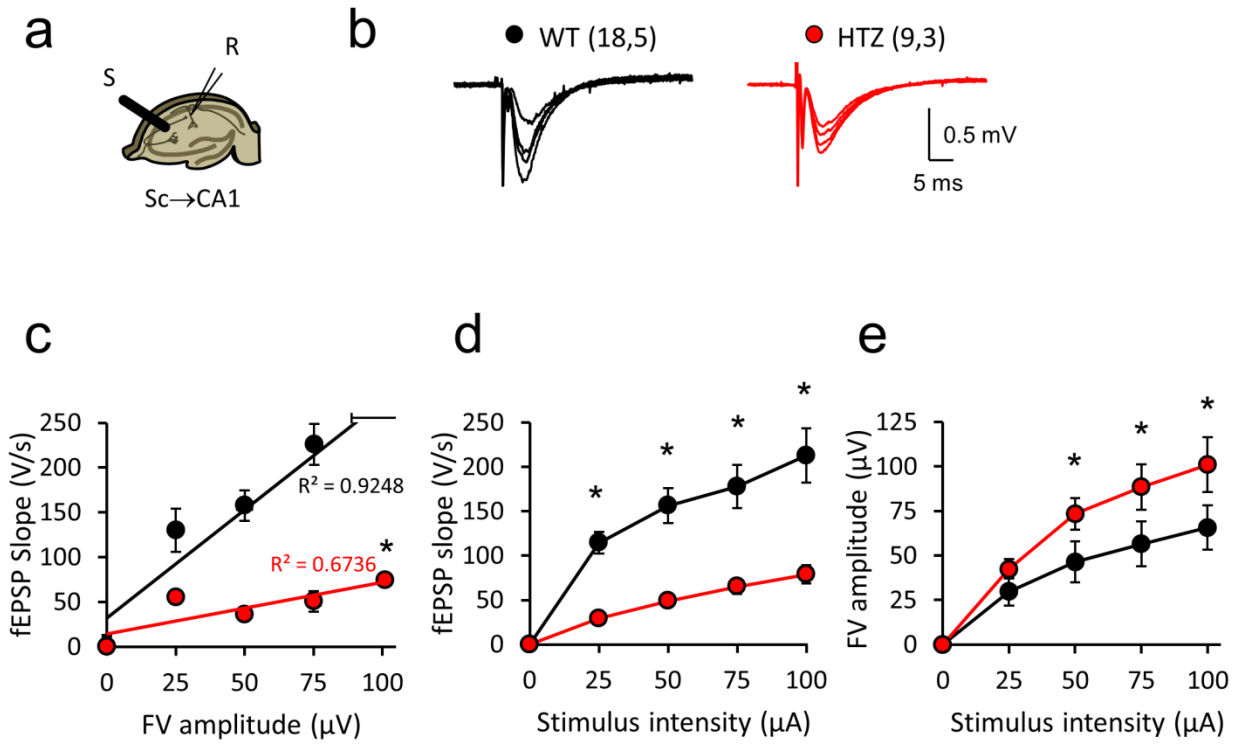

Figure 2: Impaired basal excitatory synaptic transmission in HTZ hippocampal slices **(a)** Scheme of the experimental configuration for field recordings in Schaffer Collaterals (Sc) to CA1 hippocampal synapses. The stimulation electrode and the recording electrode (R) were positioned in *stratum radiatum* of CA1. **(b)** Representative fEPSP traces of both experimental groups HTZ (red) and WT (black**).** The numbers in parentheses are slices, animals recorded. **c)** Relationship between the slope values of fEPSPs and the amplitude of FVs obtained between each experimental groups. The R^2 values for the respective linear regressions are shown. **(d)** Mean fEPSP slopes at different intensity values are plotted per each experimental group. Note the significant difference in fEPSPs as the intensity of stimulation increased between WT and HTZ slices. **(e)** Mean FV amplitudes for WT and HTZ slices. Note the significant difference in FV amplitudes between WT and HTZ slices as the stimulus intensity increased. (WT: n = 18 slices, 5 mice; HTZ: n = 9 slices, 3 mice). All data are represented as mean ± SEM. Statistical differences were calculated using a t-test, * $p < 0.0001$ compared to the WT condition.

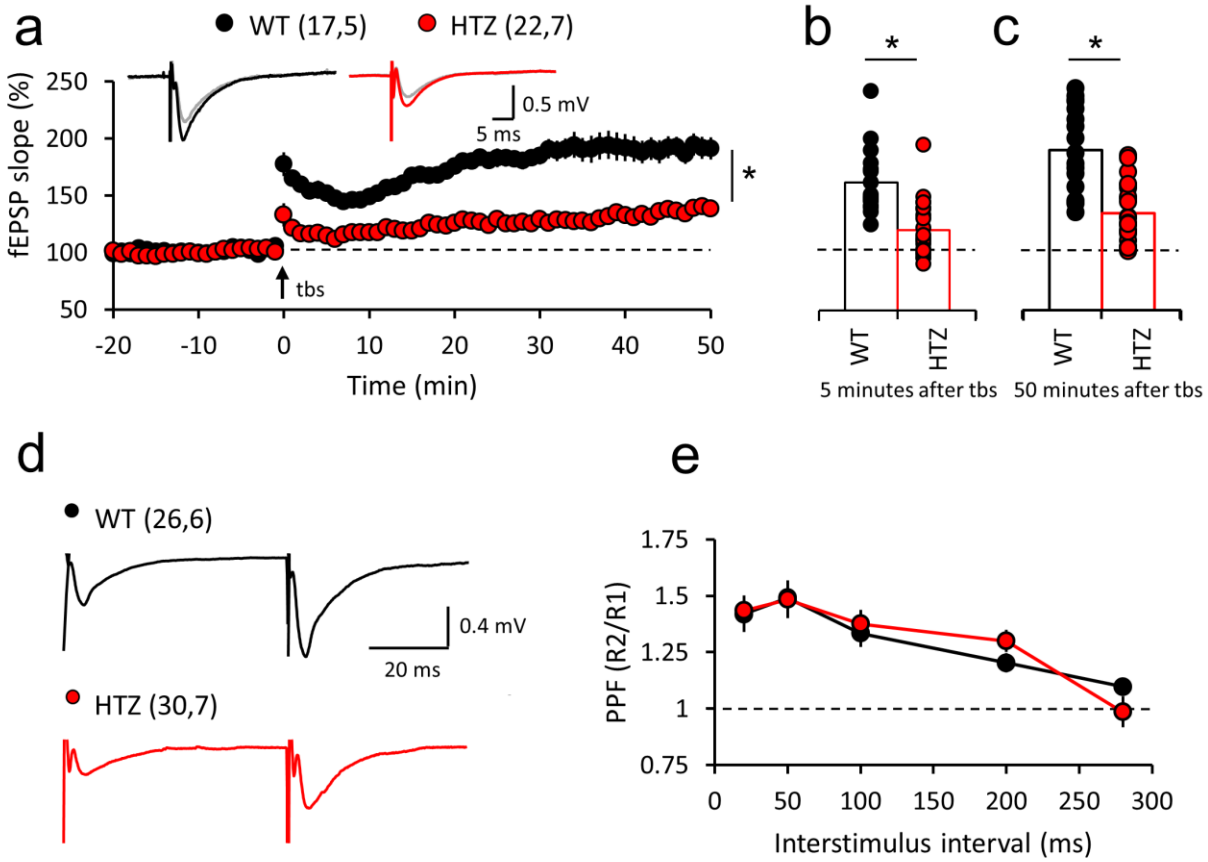

Figure 3: TBS-induced LTP impairment in excitatory synapses of HTZ hippocampal slices. **(a-c)** Hippocampal slices of 6 m.o of WT (black circles) and HTZ (red circles) mice were stimulated with a standard TBS protocol to induce LTP and excitatory postsynaptic field potentials (fEPSP) were recorded during 50 min after the application of the TBS protocol. 2-Way ANOVA, $F_{(1,2257)} = 1414$, *p <0.0001 followed by Bonferroni post hoc test ($p < 0.05$) compared to the WT condition. Representative traces before (gray) and after (black and red) the application of TBS are shown as inserts. Note that at the end of the recording (c), as well as after 5 min of LTP-induction (b) HTZ slices exhibited a significantly reduced potentiation of the synaptic strength compared to WT slices (WT: n = 17 slices, 5 mice; HTZ: n = 22 slices, 7 mice). Mann-Whitney test, *p <0.0001 compared to the WT condition in both 5 or 50 min after TBS. The numbers in parentheses are slices, animals recorded **(d)** Representative traces of HTZ (red) and WT (black) slices stimulated with two stimuli of the same intensity separated by a time of 50 ms for PPF index estimation. Note that the amplitude of the second response was greater than the first one in both cases. **(e)** Paired pulse facilitation by different stimulation intervals. Note that no significant differences were observed between the experimental groups (WT: n = 26, slices 6 mice; HTZ: n = 30 slices, 7 mice). All data are represented as mean ± SEM.

602

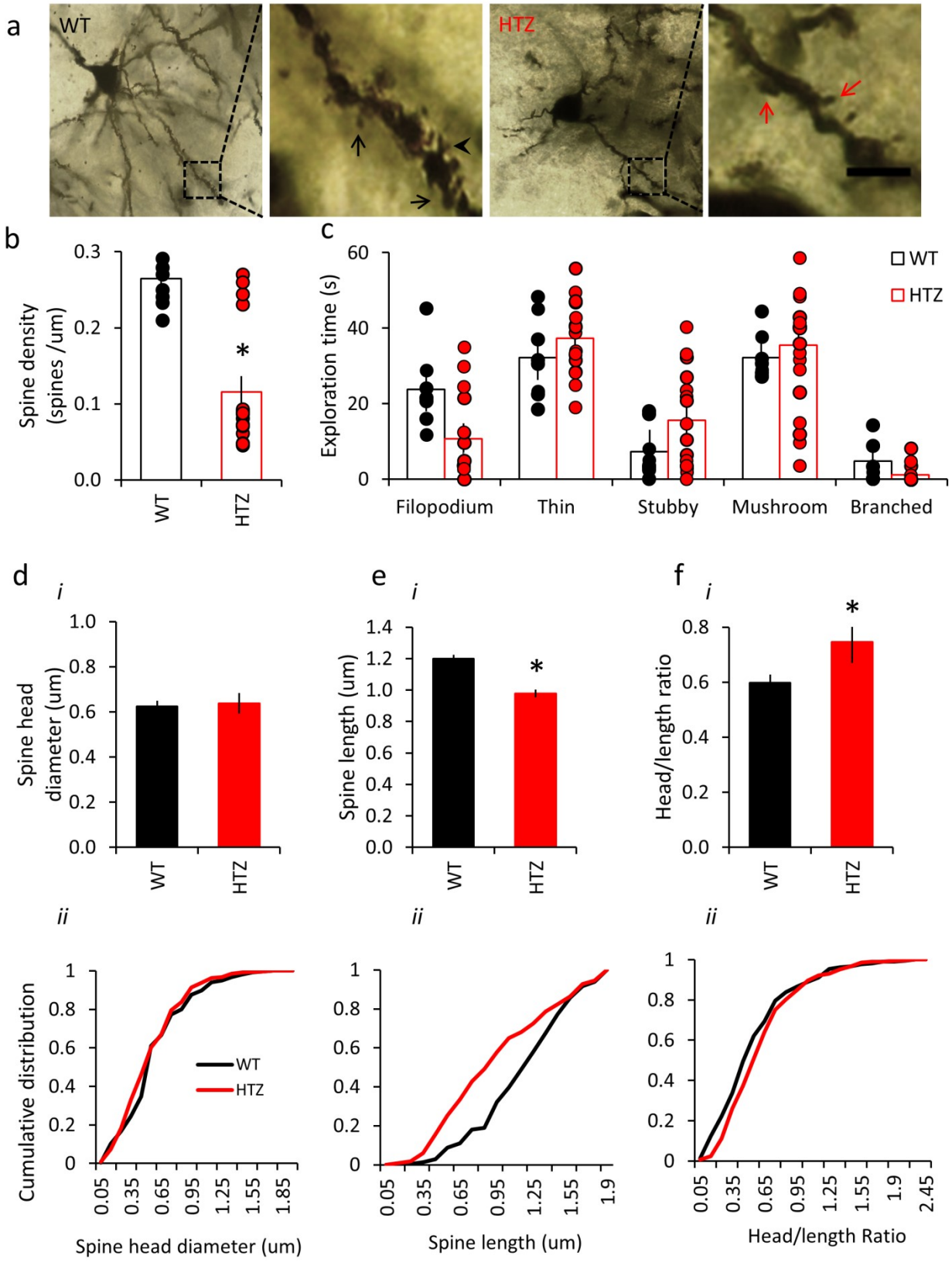
a
WT
HTZ
b
Spine density (spines /um)
0.3
0.2
0.1
0.0
*
WT
HTZ
c
Exploration time (s)
60
40
20
0
WT
HTZ
Filopodium
Thin
Stubby
Mushroom
Branched
d
i
Spine head diameter (um)
1.0
0.8
0.6
0.4
0.2
0.0
WT
HTZ
ii
Cumulative distribution
1
0.8
0.6
0.4
0.2
0
WT
HTZ
0.05
0.35
0.65
0.95
1.25
1.55
1.85
Spine head diameter (um)
e
i
Spine length (um)
1.4
1.2
1.0
0.8
0.6
0.4
0.2
0.0
*
WT
HTZ
ii
1
0.8
0.6
0.4
0.2
0
0.05
0.35
0.65
0.95
1.25
1.55
1.9
Spine length (um)
f
i
Head/length ratio
0.8
0.6
0.4
0.2
0.0
*
WT
HTZ
ii
1
0.8
0.6
0.4
0.2
0
0.05
0.35
0.65
0.95
1.25
1.55
1.9
2.45
Head/length Ratio

603

Figure 4: Reduced spine density and spine length in hippocampal neurons from adult HTZ brains. Brains from WT (black bars) and HTZ (red bars) mice over 6 m.o were isolated and Golgi-stained for visualization of pyramidal hippocampal neurons **(a)** Representative neurons and dendritic shafts per genotype. Black and red arrows point spines in WT and HTZ dendrites respectively. Black arrowhead highlights a branched spine. Scale bar= 2.5 µm **(b)** Mean spine density per neuron (number of spines per 1 µm of dendritic segment) **(c)** Mean percentage of filopodium, thin, stubby, mushroom and branched spines in WT and HTZ hippocampal neurons. 4 dendritic shafts per neuron were analyzed. N=8 WT neurons and 19 HTZ neurons from at least 2 different animals per genotype. Bars are mean ± SEM **(d-f)** Average (i) and cumulative distribution (ii) of spine head diameters (d), spine lengths (e) and head/length ratios (f) in WT and HTZ Golgi-stained neurons. N=217 WT spines, 332 HTZ spines. *$p<0.005$ versus WT condition, Mann-Whitney 2-tail test for non-parametric data.

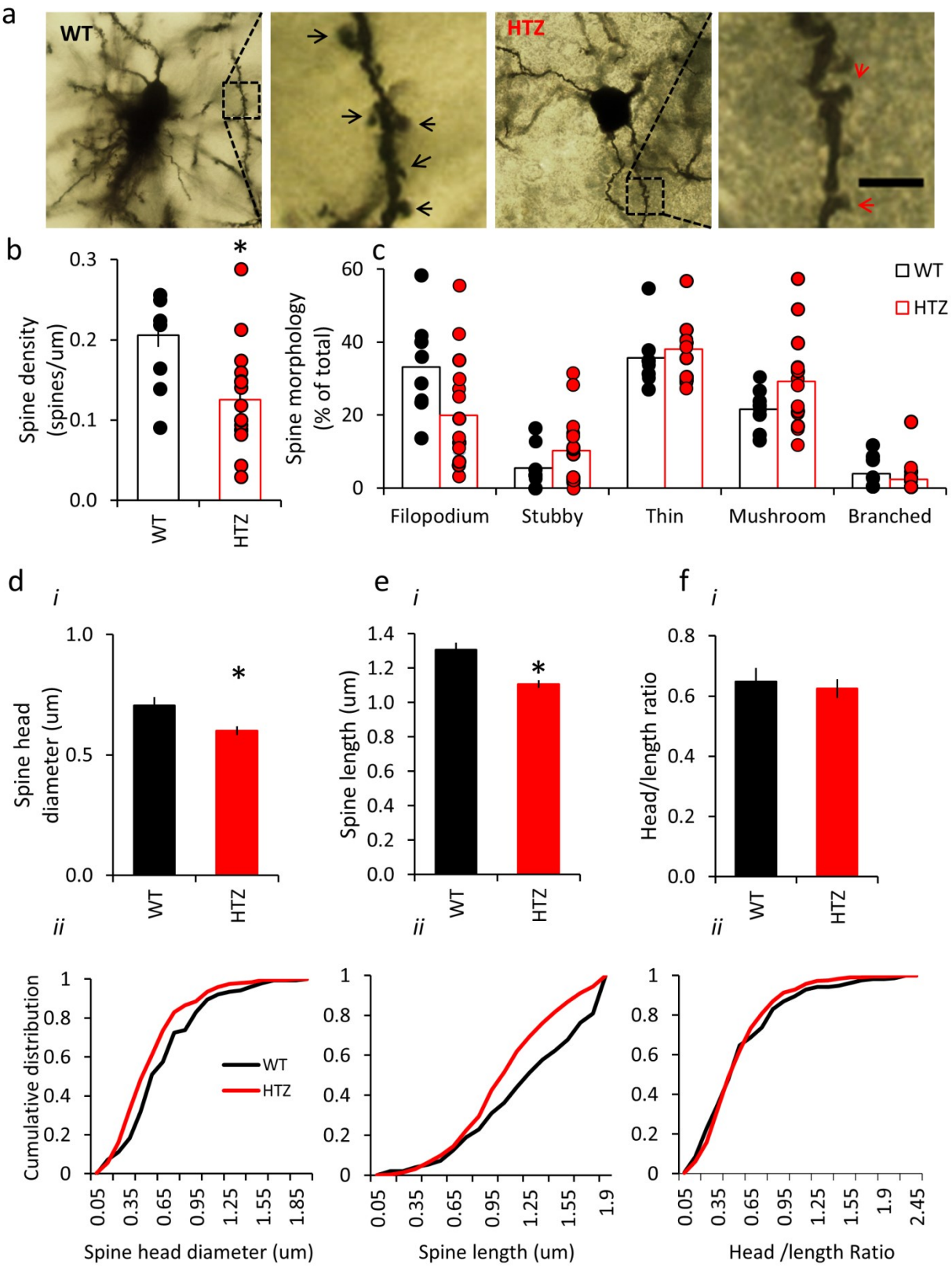
a
WT
HTZ
b
Spine density (spines/um)
0.3
0.2
0.1
0.0
*
WT
HTZ
c
Spine morphology (% of total)
60
40
20
0
WT
HTZ
Filopodium
Stubby
Thin
Mushroom
Branched
d
i
Spine head diameter (um)
1.0
0.5
0.0
*
WT
HTZ
ii
Cumulative distribution
1
0.8
0.6
0.4
0.2
0
WT
HTZ
0.05
0.35
0.65
0.95
1.25
1.55
1.85
Spine head diameter (um)
e
i
Spine length (um)
1.4
1.2
1.0
0.8
0.6
0.4
0.2
0.0
*
WT
HTZ
ii
0.05
0.35
0.65
0.95
1.25
1.55
1.9
Spine length (um)
f
i
Head/length ratio
0.8
0.6
0.4
0.2
0.0
WT
HTZ
ii
0.05
0.35
0.65
0.95
1.25
1.55
1.9
2.45
Head /length Ratio

644
645

Figure 5: Reduced spine density and spine head diameter in cortical neurons from adult HTZ brains. Brains from WT (black bars) and HTZ (red bars) mice over 6 m.o were isolated and Golgi- stained for visualization of pyramidal cortical neurons **(a)** Representative neurons and dendritic shafts per genotype. Black and red arrows point spines in WT and HTZ dendrites respectively. Scale bar= 2.5 µm **(b)** Mean spine density per neuron **(c)** Mean percentage of filopodium, thin, stubby, mushroom or branched spines in WT and HTZ cortical neurons. 4 dendritic shafts per neuron were analyzed N= 8 WT neurons and 19 HTZ neurons from at least two different animals per genotype. Bars are mean ± SEM **(d-f)** Average (i) and cumulative distribution (ii) of spine head diameters (d), spine lengths (e) and head/length ratios (f) in WT and HTZ Golgi-stained neurons. N=155 WT spines, 328 HTZ spines. *$p<0.005$ versus WT condition, Mann-Whitney 2-tail test for non-parametric data.

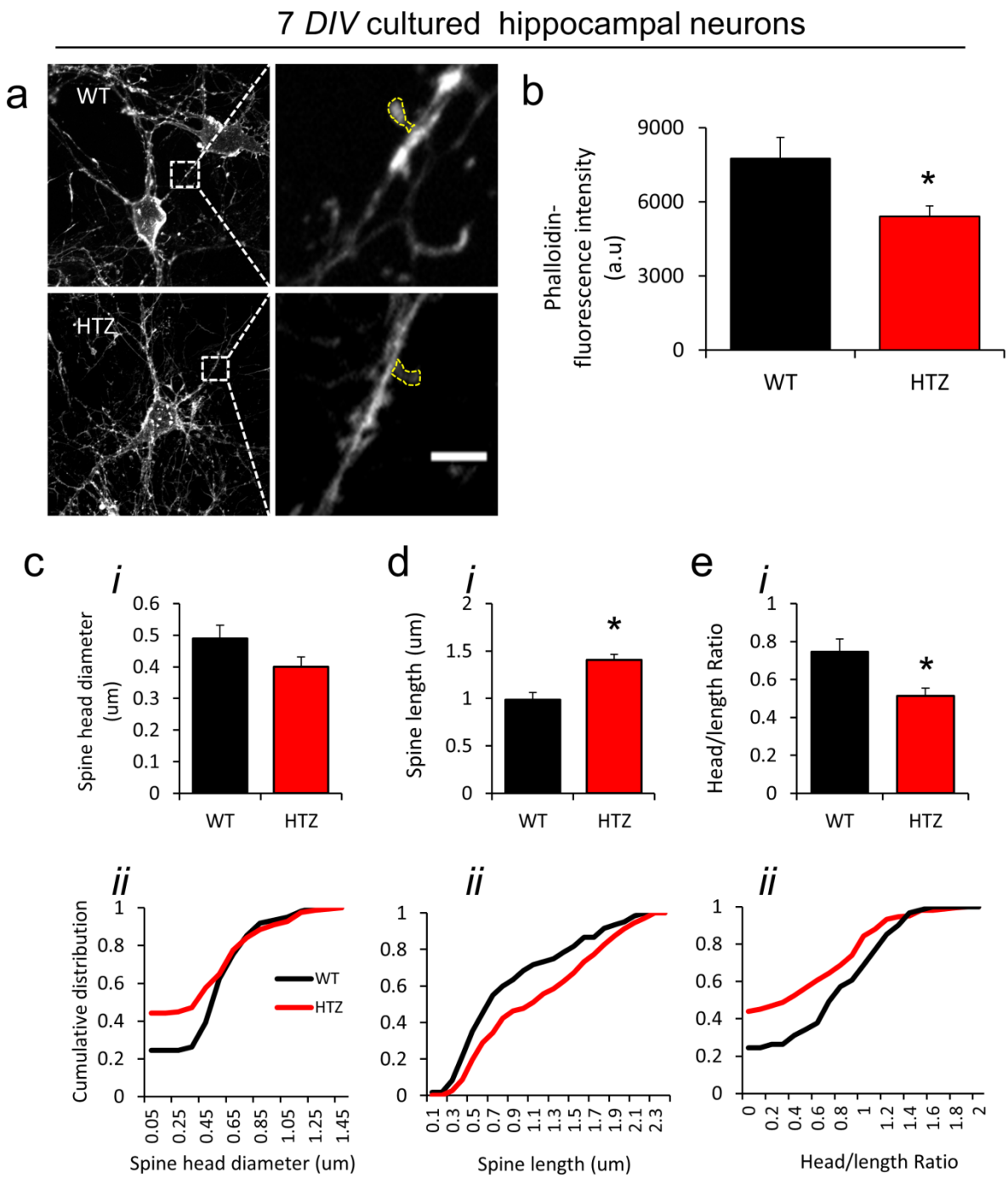
7 DIV cultured hippocampal neurons
a
WT
HTZ
b
Phalloidin-fluorescence intensity (a.u)
9000
6000
3000
0
*
WT
HTZ
c
i
Spine head diameter (um)
0.6
0.5
0.4
0.3
0.2
0.1
0
WT
HTZ
ii
Cumulative distribution
1
0.8
0.6
0.4
0.2
0
WT
HTZ
0.05
0.25
0.45
0.65
0.85
1.05
1.25
1.45
Spine head diameter (um)
d
i
Spine length (um)
2
1.5
1
0.5
0
*
WT
HTZ
ii
1
0.8
0.6
0.4
0.2
0
0.1
0.3
0.5
0.7
0.9
1.1
1.3
1.5
1.7
1.9
2.1
2.3
Spine length (um)
e
i
Head/length Ratio
1
0.8
0.6
0.4
0.2
0
*
WT
HTZ
ii
1
0.8
0.6
0.4
0.2
0
0
0.2
0.4
0.6
0.8
1
1.2
1.4
1.6
1.8
2
Head/length Ratio

Figure 6. Reduced phalloidin-reactivity in dendritic spines of HTZ neurons. 7 *DIV* hippocampal neurons, primary cultured from WT and HTZ pups (P0), were fixed, stained with the F-actin binding toxin phalloidin-rhodamin-B and visualized by confocal microscopy using comparable acquisition parameters **(a)** Representative phalloidin-stained neurons and dendritic shafts per genotype. Yellow dotted lines delimit dendritic spines inside which phalloidin-fluorescence intensity was measured. Scale bar= 2 µm. **(b)** Mean phalloidin-fluorescence intensity in WT (black bar) and HTZ (red bar) dendritic spines. N=61 WT spines and 166 HTZ from 3 WT and 18 HTZ neurons. Bars are mean ± SEM *$p<0.0002$ compared to WT condition, Mann-Whitney 2-tail test for non-parametric data. **(c-e)** Average (i) and cumulative distribution (ii) of spine head diameters (c), spine lengths (d) and head/length ratios (e) in WT and HTZ phalloidin-stained neurons. N=61 WT spines, 166 HTZ spines. *$p<0.005$ versus WT condition, Mann-Whitney 2-tail test for non-parametric data.

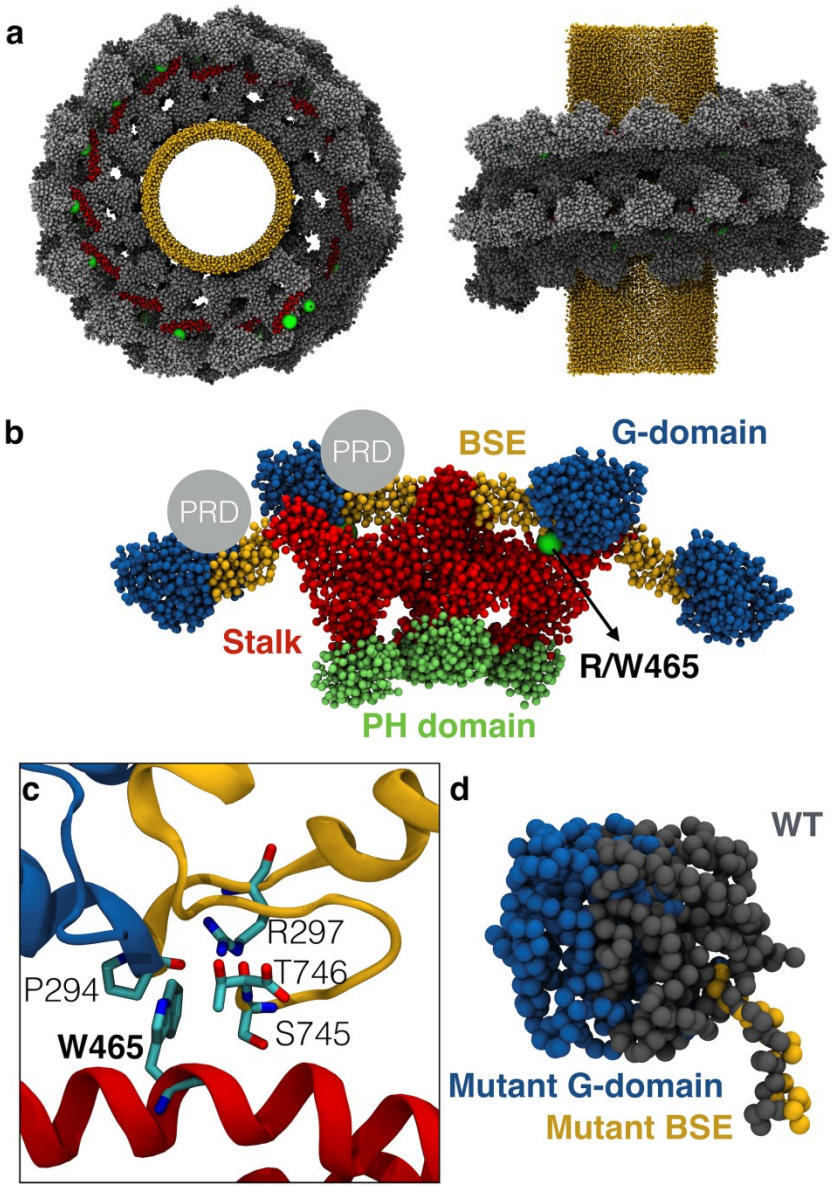

Figure 7: The CNM-causing p.R465W mutation localizes near to a putative direct actin-binding motif in dynamin-2 **(a)** Corse-grained model of a dynamin-2 helix surrounding a lipid nanotube. Dynamin-2 is represented in silver and gray; Putative actin-binding region proposed by Gu et al., (2010) (residues 399 to 444 in the middle domain) are shown in red; the residue R/W465 is represented in green and the lipid nanotube in yellow. **(b)** Tetramer configuration in the dynamin-2 helix. G-domains are colored in blue, BSEs are represented in yellow, stalks are shown in red and PH domains in lime. The position of PRD is represented only in two dynamins-2 as a silver circles. Green dot represent R/W465. **(c)** Amino acids of the BSE that are close to the R/W465. This interaction occurs in a zone close to the PRD. **(d)** G-domains and BSE of WT and mutant dynamin-2. The extension of BSE in the mutant dynamin-2 changes the position of the G-domain.

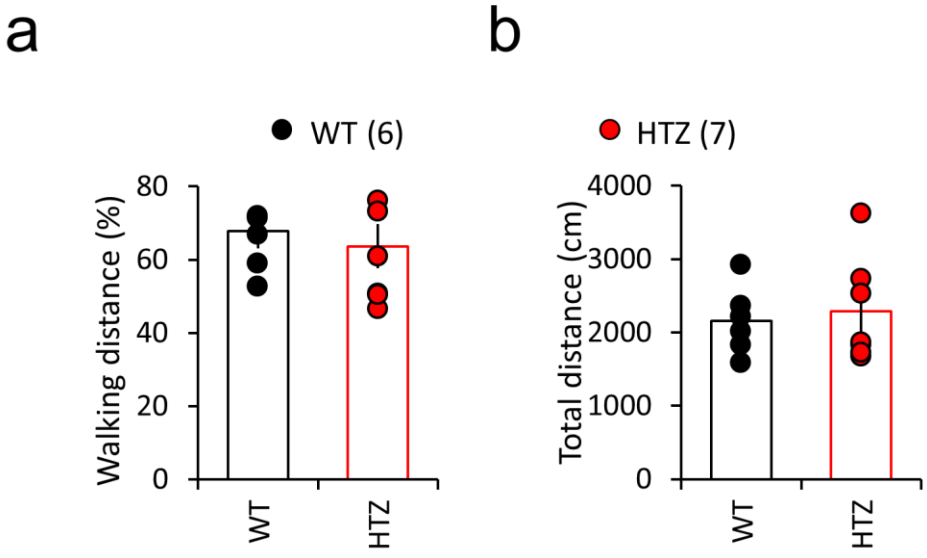
a
b
WT (6)
HTZ (7)
Walking distance (%)
80
60
40
20
0
WT
HTZ
Total distance (cm)
4000
3000
2000
1000
0
WT
HTZ

Figure S1: Locomotion activity is not different between WT and HTZ mice. WT (black circles) and HTZ (red circles) mice over 6 m.o were left to explore freely in an open field arena during 5 min. (a) Mean percentage of the walking time and (b) total distance traveled are plotted per each experimental group. All data are represented as mean ± SEM. N= 6 WT and 7 HTZ mice. Statistical differences were calculated using a non-parametric Mann-Whitney test.

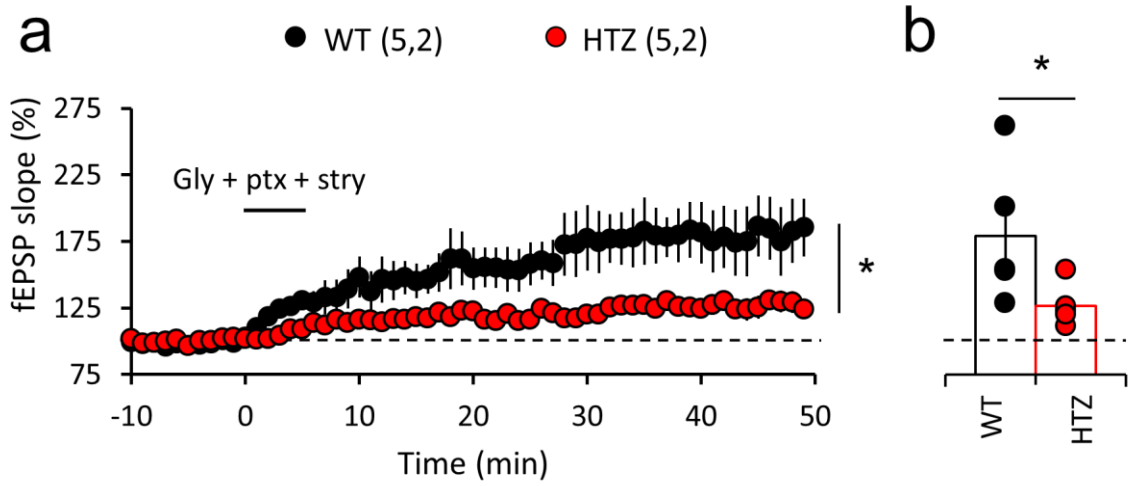

Figure S2: Impaired glycine-induced LTP in HTZ hippocampal slices. **(a-b)** Hippocampal slices from 6 m.o WT (black circles) and HTZ (red circles) mice were stimulated with the application of 600 µM glycine + 50 µM PTX + 3 µM strychnine in order to chemically induce LTP and fEPSPs were recorded during 50 min. 2-Way ANOVA, $F_{(1,480)} = 208.2$, *p <0.0001 followed by Bonferroni post hoc test ($p < 0.05$) compared to the WT condition. Note that HTZ hippocampal slices exhibit a significantly reduced potentiation at the end of the recording (b) compared to the WT slices (N= 5 slices, 2 WT mice; 5 slices, 2 HTZ mice). Mann-Whitney test * p <0.005 compared to the WT condition. All data are represented as mean ± SEM.

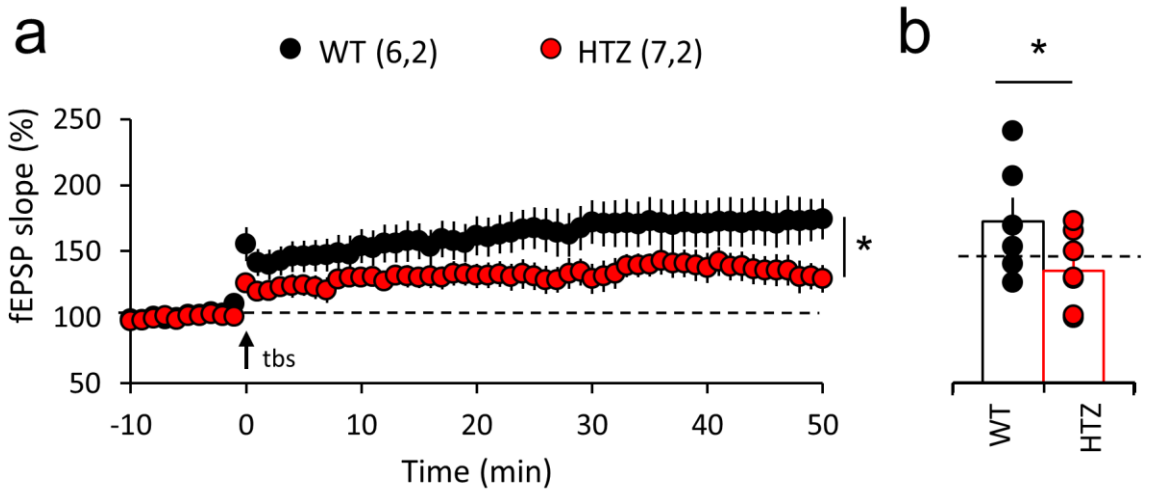

Figure S3. LTP impairment in HTZ hippocampal slices is independent of inhibitory synaptic transmission. **(a-b)** Hippocampal slices from 6 m.o WT (black circles) and HTZ (red circles) mice were stimulated with a standard TBS protocol in the presence of the GABAR-inhibitor Picrotoxin (PTX). fEPSPs were recorded during 50 min after TBS-application. 2-Way ANOVA, $F_{(1,671)} = 245.8$, *p <0.0001 followed by Bonferroni post hoc test ($p < 0.05$) compared to the WT condition. Note that even in the presence of PTX, HTZ hippocampal slices exhibit a significantly reduced potentiation compared to WT slices, suggesting that inhibitory transmission is not involved in the synaptic plasticity defects in HTZ slices. N= 6 slices, 2 WT mice/ 7 slices, 2 HTZ mice). Mann-Whitney test * p <0.005 compared to the WT condition. All data are represented as mean ± SEM.

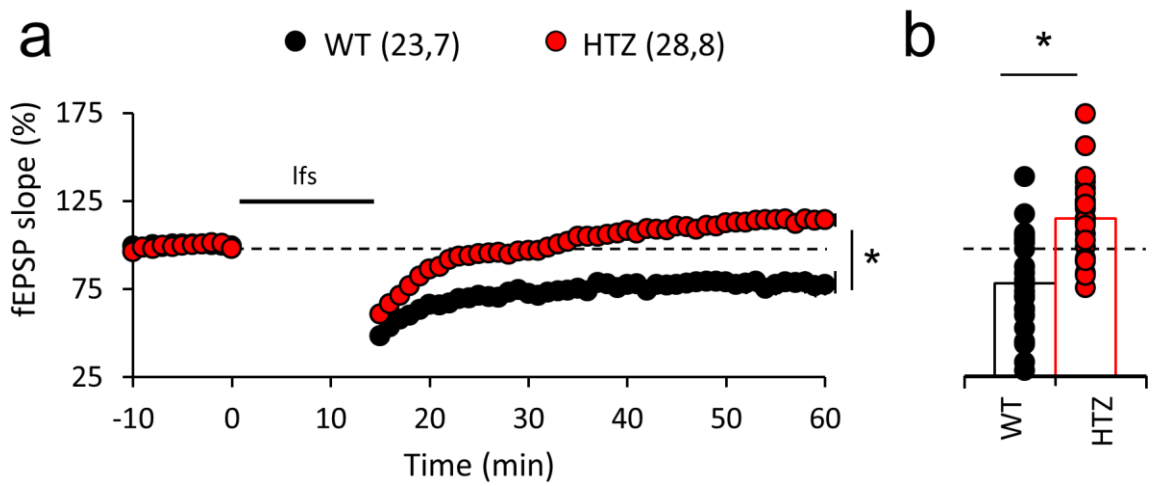

Figure S4. Impaired LFS-induced LTD in HTZ hippocampal slices. **(a-b)** Hippocampal slices from 6 m.o WT (black circles) and HTZ (red circles) mice were stimulated with a standard low-frequency electrical stimulation (LFS) protocol and fEPSPs were recorded during 60 min to estimate depression of the synaptic response (LTD). 2-Way ANOVA, $F_{(1,2793)} = 1039$, *p <0.0001 followed by Bonferroni post hoc test ($p < 0.05$) compared to the WT condition. Note that HTZ hippocampal slices exhibit a significantly reduced capability to depress the synaptic response at the end of the recording compared to WT slices (WT: n = 23 slices, 7 mice; HTZ: n = 28 slices, 8 mice). Mann-Whitney test * p <0.005 compared to the WT condition. All data are represented as mean ± SEM.

.

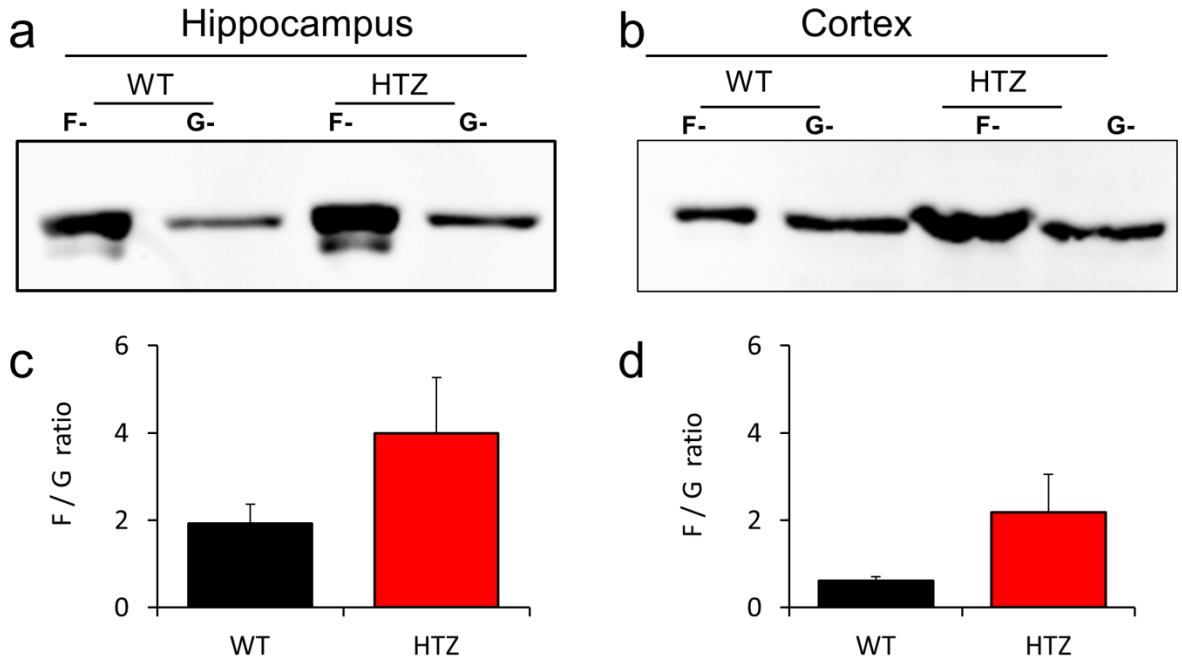

Figure S5: Imbalance in the F/G actin ratio in brains of HTZ mice. Representative blots of the relative amounts of F- and G-actin in the hippocampus (a) and cortex (b) of WT and HTZ mice are shown. (c-d) Graphs summarize the quantification of the densitometry analysis of the F/G actin ratio in hippocampus (c) and cortex (d) isolated from WT and HTZ mouse brains. Bars are mean ± SEM of tissues from 3 WT and 3 HTZ mice. Statistical comparison was done using Mann-Whitney test for non-parametric data. p=0.200 and 0.400 for hippocampus and cortex, respectively. Although not significant , HTZ brain tissues tended to exhibit an increased F/G ratio compared to the WT condition.

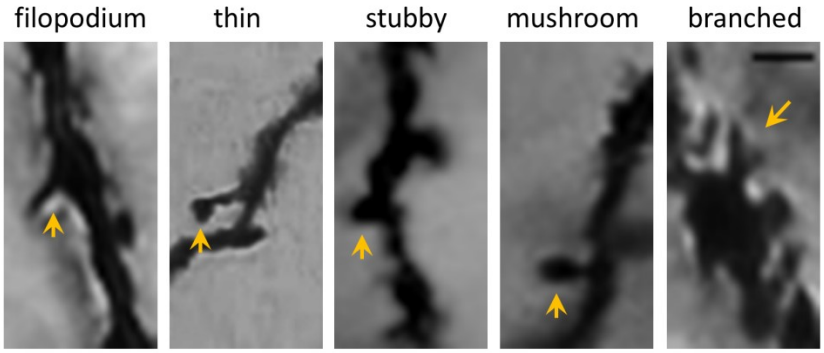

Figure S6. Representative dendritic spine-morphologies. Filopodia are long protrusions (> 2 um) without head. Thin-spines are short (<2 um) protrusions with small heads (<0.5 um). Stubby-spines are wide-head protrusions without neck. Mushroom spines are short protrusions (<1 um) with wide-heads (> 0.6 um width). Branched spines are short cup-shaped protrussions. Yellow arrows point dendritic spines of each morphology. Scale bar=2 um

References

Ali, Tayyibah, Joanna Bednarska, Stéphane Vassilopoulos, Martin Tran, Ivan A. Diakonov, Azza Ziyadeh-Isleem, Pascale Guicheney, et al. 2019. "Correlative SICM-FCM Reveals Changes in Morphology and Kinetics of Endocytic Pits Induced by Disease-Associated Mutations in Dynamin." *FASEB Journal* 33 (7): 8504–18. https://doi.org/10.1096/fj.201802635R.

Anggono, Victor, and Richard L. Huganir. 2012a. "Regulation of AMPA Receptor Trafficking and Synaptic Plasticity." *Current Opinion in Neurobiology*. Curr Opin Neurobiol. https://doi.org/10.1016/j.conb.2011.12.006.

2012b. "Regulation of AMPA Receptor Trafficking and Synaptic Plasticity." *Current Opinion in Neurobiology*. Curr Opin Neurobiol. https://doi.org/10.1016/j.conb.2011.12.006.

Antonny, Bruno, Christopher Burd, Pietro De Camilli, Elizabeth Chen, Oliver Daumke, Katja Faelber, Marijn Ford, et al. 2016. "Membrane Fission by Dynamin: What We Know and What We Need to Know." *The EMBO Journal*. https://doi.org/10.15252/embj.201694613.

Ardiles, Alvaro O., Carolina Flores-Muñoz, Gabriela Toro-Ayala, Ana M. Cárdenas, Adrian G. Palacios, Pablo Muñoz, Marco Fuenzalida, Juan C. Sáez, and Agustín D. Martínez. 2014. "Pannexin 1 Regulates Bidirectional Hippocampal Synaptic Plasticity in Adult Mice." *Frontiers in Cellular Neuroscience* 8 (OCT). https://doi.org/10.3389/fncel.2014.00326.

Arriagada-Diaz, Jorge, Lorena Prado-Vega, Ana M. Cárdenas Díaz, Alvaro O. Ardiles, and Arlek M. Gonzalez-Jamett. 2020. "Dynamin Superfamily at Pre- and Postsynapses: Master Regulators of Synaptic Transmission and Plasticity in Health and Disease." *Neuroscientist*. SAGE Publications Inc. https://doi.org/10.1177/1073858420974313.

Barnes, C. A. 1979. "Memory Deficits Associated with Senescence: A Neurophysiological and Behavioral Study in the Rat." *Journal of Comparative and Physiological Psychology*. https://doi.org/10.1037/h0077579.

Bayazitov, Ildar T., Robert J. Richardson, Robert G. Fricke, and Stanislav S. Zakharenko. 2007. "Slow Presynaptic and Fast Postsynaptic Components of Compound Long-Term Potentiation." *Journal of Neuroscience* 27 (43): 11510–21. https://doi.org/10.1523/JNEUROSCI.3077-07.2007.

Bhatnagar, Anushree, David L. Willins, John A. Gray, Jason Woods, Jeffrey L. Benovic, and Bryan L. Roth. 2001. "The Dynamin-Dependent, Arrestin-Independent Internalization of 5-Hydroxytryptamine 2A (5-HT2A) Serotonin Receptors Reveals Differential Sorting of Arrestins and 5-HT2A Receptors during Endocytosis." *Journal of Biological Chemistry*. https://doi.org/10.1074/jbc.M006968200.

Bhatnagar, Anushree, David L Willins, John A Gray, Jason Woods, Jeffrey L Benovic, and Bryan L Roth. 2000. "The Dynamin-Dependent, Arrestin-Independent Internalization of 5-Hydroxytryptamine 2A (5-HT 2A) Serotonin Receptors Reveals Differential Sorting of Arrestins and 5-HT 2A Receptors during Endocytosis* □ S." *THE JOURNAL OF BIOLOGICAL CHEMISTRY* 276 (11): 8269–77. https://doi.org/10.1074/jbc.M006968200.

Bitoun, Marc, Svetlana Maugenre, Pierre Yves Jeannet, Emmanuelle Lacène, Xavier Ferrer, Pascal Laforêt, Jean Jacques Martin, et al. 2005. "Mutations in Dynamin 2 Cause Dominant Centronuclear

930 Myopathy." *Nature Genetics*. https://doi.org/10.1038/ng1657.

931 Bliek, A. M. Van der, T. E. Redelmeier, H. Damke, E. J. Tisdale, E. M. Meyerowitz, and S. L. Schmid. 1993.
932 "Mutations in Human Dynamin Block an Intermediate Stage in Coated Vesicle Formation." *Journal*
933 *of Cell Biology*. https://doi.org/10.1083/jcb.122.3.553.

934 Böhm, Johann, Valerie Biancalana, Elizabeth T. DeChene, Marc Bitoun, Christopher R. Pierson, Elise
935 Schaefer, Hatice Karasoy, et al. 2012. "Mutation Spectrum in the Large Gtpase Dynamin 2, and
936 Genotype-Phenotype Correlation in Autosomal Dominant Centronuclear Myopathy." *Human*
937 *Mutation*. https://doi.org/10.1002/humu.22067.

938 Bosch, Miquel, Jorge Castro, Takeo Saneyoshi, Hitomi Matsuno, Mriganka Sur, and Yasunori Hayashi.
939 2014. "Structural and Molecular Remodeling of Dendritic Spine Substructures during Long-Term
940 Potentiation." *Neuron* 82 (2): 444–59. https://doi.org/10.1016/j.neuron.2014.03.021.

941 Bosch, Miquel, and Yasunori Hayashi. 2012. "Structural Plasticity of Dendritic Spines." *Current Opinion in*
942 *Neurobiology*. Elsevier Current Trends. https://doi.org/10.1016/j.conb.2011.09.002.

943 Carroll, Reed C., Eric C. Beattie, Houhui Xia, Christian Lüscher, Yoram Altschuler, Roger A. Nicoll, Robert
944 C. Malenka, and Mark Von Zastrow. 1999. "Dynamin-Dependent Endocytosis of Ionotropic
945 Glutamate Receptors." *Proceedings of the National Academy of Sciences of the United States of*
946 *America*. https://doi.org/10.1073/pnas.96.24.14112.

947 Chappie, Joshua S., Sharmistha Acharya, Ya Wen Liu, Marilyn Leonard, Thomas J. Pucadyil, and Sandra L.
948 Schmid. 2009. "An Intramolecular Signaling Element That Modulates Dynamin Function in Vitro
949 and in Vivo." *Molecular Biology of the Cell*. https://doi.org/10.1091/mbc.E09-04-0318.

950 Cheung, Giselle, and Michael A. Cousin. 2019. "Synaptic Vesicle Generation from Activity-Dependent
951 Bulk Endosomes Requires a Dephosphorylation-Dependent Dynamin–Syndapin Interaction."
952 *Journal of Neurochemistry* 151 (5): 570–83. https://doi.org/10.1111/jnc.14862.

953 Chowdhury, Shoaib, Jason D. Shepherd, Hiroyuki Okuno, Gregory Lyford, Ronald S. Petralia, Niels Plath,
954 Dietmar Kuhl, Richard L. Huganir, and Paul F. Worley. 2006. "Arc/Arg3.1 Interacts with the
955 Endocytic Machinery to Regulate AMPA Receptor Trafficking." *Neuron* 52 (3): 445–59.
956 https://doi.org/10.1016/j.neuron.2006.08.033.

957 Cingolani, Lorenzo A., Agnes Thalhammer, Lily M.Y. Yu, Myriam Catalano, Timothy Ramos, Michael A.
958 Colicos, and Yukiko Goda. 2008. "Activity-Dependent Regulation of Synaptic AMPA Receptor
959 Composition and Abundance by B3 Integrins." *Neuron* 58 (5): 749–62.
960 https://doi.org/10.1016/j.neuron.2008.04.011.

961 Citri, Ami, and Robert C. Malenka. 2008. "Synaptic Plasticity: Multiple Forms, Functions, and
962 Mechanisms." *Neuropsychopharmacology*. Neuropsychopharmacology.
963 https://doi.org/10.1038/sj.npp.1301559.

964 Damke, Hanna, Takeshi Baba, Dale E. Warnock, and Sandra L. Schmid. 1994. "Induction of Mutant
965 Dynamin Specifically Blocks Endocytic Coated Vesicle Formation." *Journal of Cell Biology*.
966 https://doi.org/10.1083/jcb.127.4.915.

967 Durieux, Anne Cécile, Bernard Prudhon, Pascale Guicheney, and Marc Bitoun. 2010. "Dynamin 2 and
968 Human Diseases." *Journal of Molecular Medicine*. https://doi.org/10.1007/s00109-009-0587-4.

969 Durieux, Anne Cécile, Stéphane Vassilopoulos, Jeanne Lainé, Bodvaël Fraysse, Laura Briñas, Bernard
970 Prudhon, Josiane Castells, et al. 2012. "A Centronuclear Myopathy - Dynamin 2 Mutation Impairs
971 Autophagy in Mice." *Traffic* 13 (6): 869–79. https://doi.org/10.1111/j.1600-0854.2012.01348.x.

972 Durieux, Anne Cécile, Alban Vignaud, Bernard Prudhon, Mai Thao Viou, Maud Beuvin, Stéphane
973 Vassilopoulos, Bodvaël Fraysse, et al. 2010. "A Centronuclear Myopathy-Dynamin 2 Mutation
974 Impairs Skeletal Muscle Structure and Function in Mice." *Human Molecular Genetics*.
975 https://doi.org/10.1093/hmg/ddq413.

976 Echaniz-Laguna, Andoni, Anne Sophie Nicot, Sophie Carré, Jérôme Franques, Christine Tranchant,
977 Nicolas Dondaine, Valérie Biancalana, Jean Louis Mandel, and Jocelyn Laporte. 2007. "Subtle
978 Central and Peripheral Nervous System Abnormalities in a Family with Centronuclear Myopathy
979 and a Novel Dynamin 2 Gene Mutation." *Neuromuscular Disorders*.
980 https://doi.org/10.1016/j.nmd.2007.06.467.

981 Ennaceur, A., and J. Delacour. 1988. "A New One-Trial Test for Neurobiological Studies of Memory in
982 Rats. 1: Behavioral Data." *Behavioural Brain Research* 31 (1): 47–59. https://doi.org/10.1016/0166-
983 4328(88)90157-X.

984 Fa, Mauro, Agnieszka Staniszewski, Faisal Saeed, Yitshak I. Francis, and Ottavio Arancio. 2014. "Dynamin
985 1 Is Required for Memory Formation." *PLoS ONE* 9 (3).
986 https://doi.org/10.1371/journal.pone.0091954.

987 Faelber, Katja, York Posor, Song Gao, Martin Held, Yvette Roske, Dennis Schulze, Volker Haucke, Frank
988 Noé, and Oliver Daumke. 2011. "Crystal Structure of Nucleotide-Free Dynamin." *Nature*.
989 https://doi.org/10.1038/nature10369.

990 Ferguson, Shawn M., Gabor Brasnjo, Mitsuko Hayashi, Markus Wölfel, Chiara Collesi, Silvia Giovedi,
991 Andrea Raimondi, et al. 2007. "A Selective Activity-Dependent Requirement for Dynamin 1 in
992 Synaptic Vesicle Endocytosis." *Science*. https://doi.org/10.1126/science.1140621.

993 Ferguson, Shawn M., and Pietro De Camilli. 2012. "Dynamin, a Membrane-Remodelling GTPase." *Nature*
994 *Reviews Molecular Cell Biology*. https://doi.org/10.1038/nrm3266.

995 Ferguson, Shawn, Andrea Raimondi, Summer Paradise, Hongying Shen, Kumi Mesaki, Agnes Ferguson,
996 Olivier Destaing, et al. 2009. "Coordinated Actions of Actin and BAR Proteins Upstream of Dynamin
997 at Endocytic Clathrin-Coated Pits." *Developmental Cell*.
998 https://doi.org/10.1016/j.devcel.2009.11.005.

999 Fischer, Dirk, Muriel Herasse, Marc Bitoun, Héctor M. Barragán-Campos, Jacques Chiras, Pascal Laforêt,
1000 Michel Fardeau, Bruno Eymard, Pascale Guicheney, and Norma B. Romero. 2006. "Characterization
1001 of the Muscle Involvement in Dynamin 2-Related Centronuclear Myopathy." *Brain*.
1002 https://doi.org/10.1093/brain/awl071.

1003 Flores-Muñoz, Carolina, Bárbara Gómez, Elena Mery, Paula Mujica, Ivana Gajardo, Claudio Córdova,
1004 Daniela Lopez-Espíndola, et al. 2020. "Acute Pannexin 1 Blockade Mitigates Early Synaptic Plasticity
1005 Defects in a Mouse Model of Alzheimer's Disease." *Frontiers in Cellular Neuroscience* 14 (March).
1006 https://doi.org/10.3389/fncel.2020.00046.

1007 Ford, Marijn G.J., Simon Jenni, and Jodi Nunnari. 2011. "The Crystal Structure of Dynamin." *Nature*.
1008 https://doi.org/10.1038/nature10441.

1009 Gajardo, Ivana, Claudia S. Salazar, Daniela Lopez-Espíndola, Carolina Estay, Carolina Flores-Muñoz,
1010 Claudio Elgueta, Arlek M. Gonzalez-Jamett, Agustín D. Martínez, Pablo Muñoz, and Álvaro O.
1011 Ardiles. 2018. "Lack of Pannexin 1 Alters Synaptic GluN2 Subunit Composition and Spatial Reversal
1012 Learning in Mice." *Frontiers in Molecular Neuroscience* 11 (April).
1013 https://doi.org/10.3389/fnmol.2018.00114.

1014 Gipson, C. D., and M. F. Olive. 2017. "Structural and Functional Plasticity of Dendritic Spines – Root or
1015 Result of Behavior?" *Genes, Brain and Behavior*. Blackwell Publishing Ltd.
1016 https://doi.org/10.1111/gbb.12324.

1017 González-Jamett, Arlek M., Ximena Baez-Matus, María José Olivares, Fernando Hinostroza, Maria José
1018 Guerra-Fernández, Jacqueline Vasquez-Navarrete, Mai Thao Bui, et al. 2017. "Dynamin-2
1019 Mutations Linked to Centronuclear Myopathy Impair Actin-Dependent Trafficking in Muscle Cells."
1020 *Scientific Reports*. https://doi.org/10.1038/s41598-017-04418-w.

1021 González-Jamett, Arlek M., Fanny Momboisse, María José Guerra, Stéphane Ory, Ximena Báez-Matus,
1022 Natalia Barraza, Valerie Calco, et al. 2013. "Dynamin-2 Regulates Fusion Pore Expansion and
1023 Quantal Release through a Mechanism That Involves Actin Dynamics in Neuroendocrine
1024 Chromaffin Cells." *PLoS ONE*. https://doi.org/10.1371/journal.pone.0070638.

1025 González-Jamett, Arlek M., Fanny Momboisse, Valentina Haro-Acuña, Jorge A. Bevilacqua, Pablo
1026 Caviedes, and Ana María Cárdenas. 2013. "Dynamin-2 Function and Dysfunction along the
1027 Secretory Pathway." *Frontiers in Endocrinology*. https://doi.org/10.3389/fendo.2013.00126.

1028 Gu, Changkyu, Suma Yaddanapudi, Astrid Weins, Teresia Osborn, Jochen Reiser, Martin Pollak, John
1029 Hartwig, and Sanja Sever. 2010. "Direct Dynaming-Actin Interactions Regulate the Actin
1030 Cytoskeleton." *EMBO Journal*. https://doi.org/10.1038/emboj.2010.249.

1031 Harris, Kristen M., and S. B. Kater. 1994. "Dendritic Spines: Cellular Specializations Imparting Both
1032 Stability and Flexibility to Synaptic Function." *Annual Review of Neuroscience*. Annual Reviews Inc.
1033 https://doi.org/10.1146/annurev.ne.17.030194.002013.

1034 Hinshaw, Jenny E., and Sandra L. Schmid. 1995. "Dynamin Self-Assembles into Rings Suggesting a
1035 Mechanism for Coated Vesicle Budding." *Nature* 374 (6518): 190–92.
1036 https://doi.org/10.1038/374190a0.

1037 Holtmaat, Anthony, and Karel Svoboda. 2009. "Experience-Dependent Structural Synaptic Plasticity in
1038 the Mammalian Brain." *Nature Reviews Neuroscience*. Nat Rev Neurosci.
1039 https://doi.org/10.1038/nrn2699.

1040 Hotulainen, Pirta, and Casper C. Hoogenraad. 2010. "Actin in Dendritic Spines: Connecting Dynamics to
1041 Function." *Journal of Cell Biology* 189 (4): 619–29. https://doi.org/10.1083/jcb.201003008.

1042 Jaskolski, Frédéric, Belen Mayo-Martin, David Jane, and Jeremy M. Henley. 2009. "Dynamin-Dependent
1043 Membrane Drift Recruits AMPA Receptors to Dendritic Spines." *Journal of Biological Chemistry*.
1044 https://doi.org/10.1074/jbc.M808401200.

1045 Jeannet, P. Y., G. Bassez, B. Eymard, P. Laforêt, J. A. Urtizberea, A. Rouche, P. Guicheney, M. Fardeau,
1046 and Norma Beatriz Romero. 2004. "Clinical and Histologic Findings in Autosomal Centronuclear
1047 Myopathy." *Neurology*. https://doi.org/10.1212/01.WNL.0000124388.67003.56.

1048 Kabbani, Nadine, Andreas Jeromin, and Robert Levenson. 2004. "Dynamin-2 Associates with the
1049 Dopamine Receptor Signalplex and Regulates Internalization of Activated D2 Receptors." *Cellular*
1050 *Signalling*. https://doi.org/10.1016/j.cellsig.2003.09.011.

1051 Kim, Chong Hyun, and John E. Lisman. 1999. "A Role of Actin Filament in Synaptic Transmission and
1052 Long-Term Potentiation." *Journal of Neuroscience* 19 (11): 4314–24.
1053 https://doi.org/10.1523/jneurosci.19-11-04314.1999.

1054 Kong, Leopold, Kem A. Sochacki, Huaibin Wang, Shunming Fang, Bertram Canagarajah, Andrew D. Kehr,
1055 William J. Rice, Marie Paule Strub, Justin W. Taraska, and Jenny E. Hinshaw. 2018. "Cryo-EM of the
1056 Dynamin Polymer Assembled on Lipid Membrane." *Nature* 560 (7717): 258–62.
1057 https://doi.org/10.1038/s41586-018-0378-6.

1058 Koutsopoulos, Olga S., Catherine Koch, Valerie Tosch, Johann Böhm, Kathryn N. North, and Jocelyn
1059 Laporte. 2011. "Mild Functional Differences of Dynamin 2 Mutations Associated to Centronuclear
1060 Myopathy and Charcot-Marie-Tooth Peripheral Neuropathy." Edited by Gisela Nogales-Gadea.
1061 *PLoS ONE* 6 (11): e27498. https://doi.org/10.1371/journal.pone.0027498.

1062 Lee, Hey Kyoung, and Alfredo Kirkwood. 2011. "AMPA Receptor Regulation during Synaptic Plasticity in
1063 Hippocampus and Neocortex." *Seminars in Cell and Developmental Biology*. Elsevier Ltd.
1064 https://doi.org/10.1016/j.semcdb.2011.06.007.

1065 Lin, Shan Shan, Tsung Lin Hsieh, Gunn Guang Liou, Tsai Ning Li, Hsin Chieh Lin, Chiung Wen Chang,
1066 Hsiang Yi Wu, Chi Kuang Yao, and Ya Wen Liu. 2020. "Dynamin-2 Regulates Postsynaptic
1067 Cytoskeleton Organization and Neuromuscular Junction Development." *Cell Reports* 33 (4).
1068 https://doi.org/10.1016/j.celrep.2020.108310.

1069 Liu, Ya Wen, Vasyl Lukiyanchuk, and Sandra L. Schmid. 2011. "Common Membrane Trafficking Defects of
1070 Disease-Associated Dynamin 2 Mutations." *Traffic*. https://doi.org/10.1111/j.1600-
1071 0854.2011.01250.x.

1072 Loerke, Dinah, Marcel Mettlen, Defne Yarar, Khuloud Jaqaman, Henry Jaqaman, Gaudenz Danuser, and
1073 Sandra L. Schmid. 2009. "Cargo and Dynamin Regulate Clathrin-Coated Pit Maturation." *PLoS*
1074 *Biology*. https://doi.org/10. 1371/journal.pbio.1000057.

1075 Lomash, Richa Madan, Xinglong Gu, Richard J. Youle, Wei Lu, and Katherine W. Roche. 2015.
1076 "Neurolastin, a Dynamin Family GTPase, Regulates Excitatory Synapses and Spine Density." *Cell*
1077 *Reports* 12 (5): 743–51. https://doi.org/10.1016/j.celrep.2015.06.064.

1078 Lu, Jiuyi, Thomas D. Helton, Thomas A. Blanpied, Bence Rácz, Thomas M. Newpher, Richard J. Weinberg,
1079 and Michael D. Ehlers. 2007. "Postsynaptic Positioning of Endocytic Zones and AMPA Receptor
1080 Cycling by Physical Coupling of Dynamin-3 to Homer." *Neuron* 55 (6): 874–89.
1081 https://doi.org/10.1016/j.neuron.2007.06.041.

1082 Lu, Wei Yang, Heng Ye Man, William Ju, William S. Trimble, John F. MacDonald, and Yu Tian Wang. 2001.
1083 "Activation of Synaptic NMDA Receptors Induces Membrane Insertion of New AMPA Receptors
1084 and LTP in Cultured Hippocampal Neurons." *Neuron* 29 (1): 243–54.
1085 https://doi.org/10.1016/S0896-6273(01)00194-5.

1086 Malenka, Robert C., and Mark F. Bear. 2004. "LTP and LTD: An Embarrassment of Riches." *Neuron*.
1087 Neuron. https://doi.org/10.1016/j.neuron.2004.09.012.

1088 Matsuzaki, Masanori, Graham C.R. Ellis-Davies, Tomomi Nemoto, Yasushi Miyashita, Masamitsu Iino,
1089 and Haruo Kasai. 2001. “Dendritic Spine Geometry Is Critical for AMPA Receptor Expression in
1090 Hippocampal CA1 Pyramidal Neurons.” *Nature Neuroscience* 4 (11): 1086–92.
1091 https://doi.org/10.1038/nn736.

1092 Matus, A. 2000. “Actin-Based Plasticity in Dendritic Spines.” *Science*. Science.
1093 https://doi.org/10.1126/science.290.5492.754.

1094 Mooren, Olivia L., Tatyana I. Kotova, Andrew J. Moore, and Dorothy A. Schafer. 2009. “Dynamin2 GTPase
1095 and Cortactin Remodel Actin Filaments.” *Journal of Biological Chemistry*.
1096 https://doi.org/10.1074/jbc.M109.024398.

1097 Moro, Alessandro., van Nifterick Ann., Toonen Ruud., Verhage Matthijs. 2021. "Dynamin controls
1098 neuropeptides secretion by organizing dense-core vesicle fusion sites"Science Advances. https://DOI:
1099 10.1126/sciadv.abf0659

1100 Negrón-Oyarzo, Ignacio, David Neira, Nelson Espinosa, Pablo Fuentealba, and Francisco Aboitiz. 2015.
1101 “Prenatal Stress Produces Persistence of Remote Memory and Disrupts Functional Connectivity in
1102 the Hippocampal-Prefrontal Cortex Axis.” *Cerebral Cortex*. https://doi.org/10.1093/cercor/bhu108.

1103 Newman-Smith, Erin D., Dixie Lee Shurland, and Alexander M. Van Der Bliek. 1997. “Assignment of the
1104 Dynamin-1 Gene (DNM1) to Human Chromosome 9q34 by Fluorescence in Situ Hybridization and
1105 Somatic Cell Hybrid Analysis.” *Genomics*. https://doi.org/10.1006/geno.1996.4596.

1106 Nicoziani, Paolo, Frederik Vilhardt, Alicia Llorente, Leila Hilout, Pierre J. Courtoy, Kirsten Sandvig, and Bo
1107 Van Deurs. 2000. “Role for Dynamin in Late Endosome Dynamics and Trafficking of the Cation-
1108 Independent Mannose 6-Phosphate Receptor.” *Molecular Biology of the Cell*.
1109 https://doi.org/10.1091/mbc.11.2.481.

1110 Noakes, P. G., D. Chin, S. S. Kim, S. Liang, and W. D. Phillips. 1999. “Expression and Localisation of
1111 Dynamin and Syntaxin during Neural Development and Neuromuscular Synapse Formation.”
1112 *Journal of Comparative Neurology*. https://doi.org/10.1002/(SICI)1096-
1113 9861(19990809)410:4<531::AID-CNE2>3.0.CO;2-C.

1114 Okamoto, Ken Ichi, Takeharu Nagai, Atsushi Miyawaki, and Yasunori Hayashi. 2004. “Rapid and
1115 Persistent Modulation of Actin Dynamics Regulates Postsynaptic Reorganization Underlying
1116 Bidirectional Plasticity.” *Nature Neuroscience* 7 (10): 1104–12. https://doi.org/10.1038/nn1311.

1117 Okamoto, Kenichi, Miquel Bosch, and Yasunori Hayashi. 2009. “The Roles of CaMKII and F-Actin in the
1118 Structural Plasticity of Dendritic Spines: A Potential Molecular Identity of a Synaptic Tag?”
1119 *Physiology* 24 (6): 357–66. https://doi.org/10.1152/physiol.00029.2009.

1120 Okamoto, Patricia M., Chantal Gamby, David Wells, Justin Fallon, and Richard B. Vallee. 2001. “Dynamin
1121 Isoform-Specific Interaction with the Shank/ProSAP Scaffolding Proteins of the Postsynaptic
1122 Density and Actin Cytoskeleton.” *Journal of Biological Chemistry*.
1123 https://doi.org/10.1074/jbc.M104927200.

1124 Pelucchi, Silvia, Ramona Stringhi, and Elena Marcello. 2020. “Dendritic Spines in Alzheimer’s Disease:
1125 How the Actin Cytoskeleton Contributes to Synaptic Failure.” *International Journal of Molecular*
1126 *Sciences*. MDPI AG. https://doi.org/10.3390/ijms21030908.

1127 Penzes, Peter, and Igor Rafalovich. 2012. “Regulation of the Actin Cytoskeleton in Dendritic Spines.”
1128 *Advances in Experimental Medicine and Biology* 970: 81–95. https://doi.org/10.1007/978-3-7091-
1129 0932-8_4.

1130 Pitts, Matthew. 2018. “Barnes Maze Procedure for Spatial Learning and Memory in Mice.” *BIO-*
1131 *PROTOCOL*. https://doi.org/10.21769/bioprotoc.2744.

1132 Praefcke, Gerrit J.K., and Harvey T. McMahon. 2004. “The Dynamin Superfamily: Universal Membrane
1133 Tubulation and Fission Molecules?” *Nature Reviews Molecular Cell Biology*.
1134 https://doi.org/10.1038/nrm1313.

1135 Raimondi, Andrea, Shawn M. Ferguson, Xuelin Lou, Moritz Armbruster, Summer Paradise, Silvia Giovedi,
1136 Mirko Messa, et al. 2011. “Overlapping Role of Dynamin Isoforms in Synaptic Vesicle Endocytosis.”
1137 *Neuron*. https://doi.org/10.1016/j.neuron.2011.04.031.

1138 Romero, Norma B., and Marc Bitoun. 2011. “Centronuclear Myopathies.” *Seminars in Pediatric*
1139 *Neurology* 18 (4): 250–56. https://doi.org/10.1016/j.spen.2011.10.006.

1140 Schiffer, Mario, Beina Teng, Changkyu Gu, Valentina A. Shchedrina, Marina Kasaikina, Vincent A. Pham,
1141 Nils Hanke, et al. 2015. “Pharmacological Targeting of Actin-Dependent Dynamin Oligomerization
1142 Ameliorates Chronic Kidney Disease in Diverse Animal Models.” *Nature Medicine* 21 (6): 601–9.
1143 https://doi.org/10.1038/nm.3843.

1144 Shin, Wonchul, Lihao Ge, Gianvito Arpino, Seth A. Villarreal, Edaeni Hamid, Huisheng Liu, Wei Dong
1145 Zhao, Peter J. Wen, Hsueh Cheng Chiang, and Ling Gang Wu. 2018. “Visualization of Membrane
1146 Pore in Live Cells Reveals a Dynamic-Pore Theory Governing Fusion and Endocytosis.” *Cell* 173 (4):
1147 934-945.e12. https://doi.org/10.1016/j.cell.2018.02.062.

1148 Shors, Tracey J., and Louis D. Matzel. 1997. “Long-Term Potentiation: What’s Learning Got to Do with
1149 It?” *Behavioral and Brain Sciences*. Behav Brain Sci. https://doi.org/10.1017/S0140525X97001593.

1150 Singh, Mahaveer, Hemant R. Jadhav, and Tanya Bhatt. 2017. “Dynamin Functions and Ligands: Classical
1151 Mechanisms Behind.” *Molecular Pharmacology*. https://doi.org/10.1124/mol.116.105064.

1152 Stefen, Holly, Chanchanok Chaichim, John Power, and Thomas Fath. 2016. “Regulation of the
1153 Postsynaptic Compartment of Excitatory Synapses by the Actin Cytoskeleton in Health and Its
1154 Disruption in Disease.” *Neural Plasticity* 2016. https://doi.org/10.1155/2016/2371970.

1155 Sukoff Rizzo, Stacey J., and Jacqueline N. Crawley. 2017. “Behavioral Phenotyping Assays for Genetic
1156 Mouse Models of Neurodevelopmental, Neurodegenerative, and Psychiatric Disorders.” *Annual*
1157 *Review of Animal Biosciences*. https://doi.org/10.1146/annurev-animal-022516-022754.

1158 Tanabe, Kenji, and Kohji Takei. 2009. “Dynamic Instability of Microtubules Requires Dynamin 2 and Is
1159 Impaired in a Charcot-Marie-Tooth Mutant.” *Journal of Cell Biology*.
1160 https://doi.org/10.1083/jcb.200803153.

1161 Tanifuji, Shota, Megumi Funakoshi-Tago, Fumihito Uedas, Tadashi Kasaharas, and Sumiko Mochida.
1162 2013. “Dynamin Isoforms Decode Action Potential Firing for Synaptic Vesicle Recycling.” *Journal of*
1163 *Biological Chemistry*. https://doi.org/10.1074/jbc.M112.445874.

1164 Wang, Weisheng, Yun Yue Ju, Qi Xin Zhou, Jian Xin Tang, Meng Li, Lei Zhang, Shuo Kang, et al. 2017. “The

1165 Small GTPase Rac1 Contributes to Extinction of Aversive Memories of Drug Withdrawal by
1166 Facilitating GABAa Receptor Endocytosis in the VmPFC." *Journal of Neuroscience*.
1167 https://doi.org/10.1523/JNEUROSCI.3859-16.2017.

1168 Warnock, Dale E., Takeshi Baba, and Sandra L. Schmid. 1997. "Ubiquitously Expressed Dynamin-II Has a
1169 Higher Intrinsic GTPase Activity and a Greater Propensity for Self-Assembly than Neuronal
1170 Dynamin-I." *Molecular Biology of the Cell*. https://doi.org/10.1091/mbc.8.12.2553.

1171 Watanabe, Shigeki, Benjamin R. Rost, Marcial Camacho-Pérez, M. Wayne Davis, Berit Söhl-Kielczynski,
1172 Christian Rosenmund, and Erik M. Jorgensen. 2013. "Ultrafast Endocytosis at Mouse Hippocampal
1173 Synapses." *Nature* 504 (7479): 242–47. https://doi.org/10.1038/nature12809.

1174 Yamada, Hiroshi, Tadashi Abe, Ayano Satoh, Nana Okazaki, Shota Tago, Kinue Kobayashi, Yumi Yoshida,
1175 et al. 2013. "Stabilization of Actin Bundles by a Dynamin 1/Cortactin Ring Complex Is Necessary for
1176 Growth Cone Filopodia." *Journal of Neuroscience* 33 (10): 4514–26.
1177 https://doi.org/10.1523/JNEUROSCI.2762-12.2013.

1178 Zhang, Ruihui, Donghoon M. Lee, John R. Jimah, Nathalie Gerassimov, Changsong Yang, Sangjoon Kim,
1179 Delgermaa Luvsanjav, et al. 2020. "Dynamin Regulates the Dynamics and Mechanical Strength of
1180 the Actin Cytoskeleton as a Multifilament Actin-Bundling Protein." *Nature Cell Biology* 22 (6): 674–
1181 88. https://doi.org/10.1038/s41556-020-0519-7.

1182 Zhang, Xiao Yan, Fang Ji, Ning Wang, Lin Lin Chen, Tian Tian, and Wei Lu. 2014. "Glycine Induces
1183 Bidirectional Modifications in N-Methyl-D-Aspartate Receptor-Mediated Synaptic Responses in
1184 Hippocampal CA1 Neurons." *Journal of Biological Chemistry* 289 (45): 31200–211.
1185 https://doi.org/10.1074/jbc.M114.570630.

1186 Zheng, Ning, Okunola Jeyifous, Charlotte Munro, Johanna M. Montgomery, and William N. Green. 2015.
1187 "Synaptic Activity Regulates AMPA Receptor Trafficking through Different Recycling Pathways."
1188 *ELife* 4 (MAY). https://doi.org/10.7554/eLife.06878.

1189 Züchner, Stephan, Maher Noureddine, Marina Kennerson, Kristien Verhoeven, Kristl Claeys, Peter De
1190 Jonghe, John Merory, et al. 2005. "Mutations in the Pleckstrin Homology Domain of Dynamin 2
1191 Cause Dominant Intermediate Charcot-Marie-Tooth Disease." *Nature Genetics*.
1192 https://doi.org/10.1038/ng1514.

1193 Zucker, Robert S., and Wade G. Regehr. 2002. "Short-Term Synaptic Plasticity." *Annual Review of*
1194 *Physiology*. Annu Rev Physiol. https://doi.org/10.1146/annurev.physiol.64.092501.114547.

1195

1196

1197

1198

1199

1200